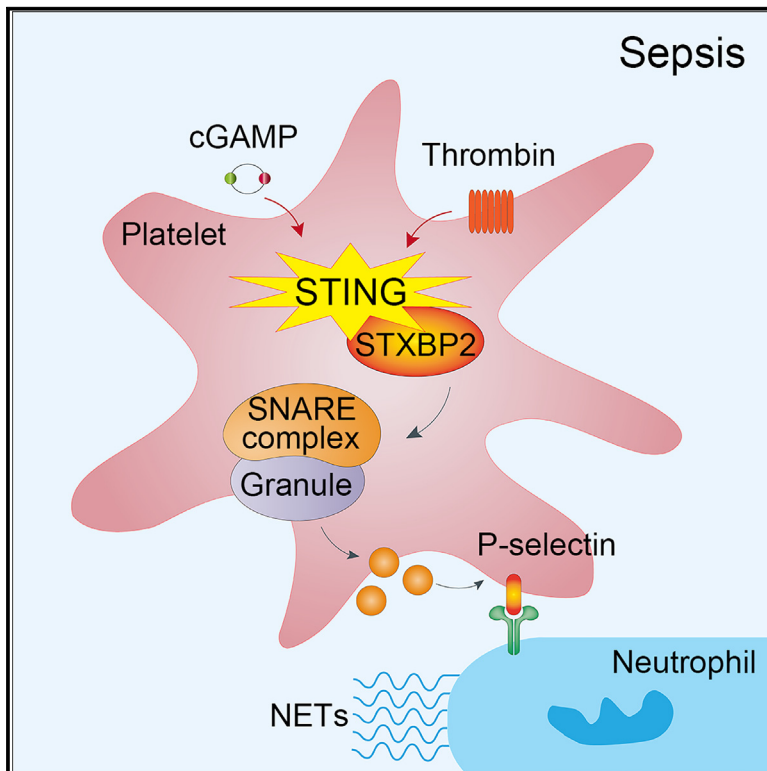


Immunity

STING activation in platelets aggravates septic thrombosis by enhancing platelet activation and granule secretion

Graphical abstract



Authors

Mina Yang, Haojie Jiang, Chen Ding, ...,
Liufu Deng, Junling Liu, Yanyan Xu

Correspondence

j4hxxx@sjtu.edu.cn (H.J.),
liujl@shsmu.edu.cn (J.L.),
xuyanyan901@shsmu.edu.cn (Y.X.)

In brief

Identifying mechanisms of platelet activation would improve our limited understanding of septic-induced coagulopathy. Yang et al. reveal that the DNA sensor, STING, in platelets promotes their granule secretion, which drives subsequent septic thrombosis. Furthermore, this work identifies a STING-STXBP2 interaction as a potential target for sepsis interventions.

Highlights

- STING deficiency in platelets suppresses platelet activation
- STING deficiency in platelets prevents NET formation during sepsis
- cGAMP promotes granule release by strengthening binding of STING to STXBP2
- The peptide C-ST5 inhibits platelet activation and excessive septic thrombosis

Article

STING activation in platelets aggravates septic thrombosis by enhancing platelet activation and granule secretion

Mina Yang,^{1,5} Haojie Jiang,^{1,5,*} Chen Ding,¹ Lin Zhang,¹ Nan Ding,¹ Guoming Li,¹ Fei Zhang,² Jing Wang,³ Liufu Deng,⁴ Junling Liu,^{1,*} and Yanyan Xu^{1,6,*}

¹Department of Biochemistry and Molecular Cell Biology, Key Laboratory of Cell Differentiation and Apoptosis of Chinese Ministry of Education, Shanghai Jiao Tong University School of Medicine, Shanghai 200025, China

²Key Laboratory of Cell Differentiation and Apoptosis of Chinese Ministry of Education, Shanghai Jiao Tong University School of Medicine, Shanghai 200025, China

³Shanghai Institute of Immunology, Department of Immunology and Microbiology, Key Laboratory of Cell Differentiation and Apoptosis of Chinese Ministry of Education, Shanghai Jiao Tong University School of Medicine, Shanghai 200025, China

⁴School of Pharmacy, Shanghai Jiao Tong University, Shanghai 200240, China

⁵These authors contributed equally

⁶Lead contact

*Correspondence: j4hhhh@sjtu.edu.cn (H.J.), liujl@shsmu.edu.cn (J.L.), xuyanyan901@shsmu.edu.cn (Y.X.)

<https://doi.org/10.1016/j.immuni.2023.02.015>

SUMMARY

Sepsis is a dysregulated inflammatory consequence of systemic infection. As a result, excessive platelet activation leads to thrombosis and coagulopathy, but we currently lack sufficient understanding of these processes. Here, using the cecal ligation and puncture (CLP) model of sepsis, we observed septic thrombosis and neutrophil extracellular trap formation (NETosis) within the mouse vasculature by intravital microscopy. STING activation in platelets was a critical driver of sepsis-induced pathology. Platelet-specific STING deficiency suppressed platelet activation and granule secretion, which alleviated sepsis-induced intravascular thrombosis and NETosis in mice. Mechanistically, sepsis-derived cGAMP promoted the binding of STING to STXBP2, the assembly of SNARE complex, granule secretion, and subsequent septic thrombosis, which probably depended on the palmitoylation of STING. We generated a peptide, C-ST5, to block STING binding to STXBP2. Septic mice treated with C-ST5 showed reduced thrombosis. Overall, platelet activation via STING reveals a potential strategy for limiting life-threatening sepsis-mediated coagulopathy.

INTRODUCTION

Sepsis is a clinically challenging systemic inflammatory response syndrome (SIRS) caused by bacterial infection.¹ Septic patients are at a high risk of developing infectious shock, disseminated intravascular coagulation (DIC), and multiple organ dysfunction syndrome (MODS).^{2,3} As a common complication of sepsis, thrombosis and coagulopathy are responsible for acute lung injury (ALI), acute kidney injury (AKI), multiple organ failure, and ultimately high mortality in sepsis patients.^{4,5}

Platelets, which are shed during the maturation of megakaryocytes, maintain homeostasis of the coagulation system.⁶ In addition to their roles in hemostasis, platelets also perform innate immune defense against infection and contribute to inflammation.⁷ During sepsis, platelets are activated by invading pathogens or inflammatory factors and then interact with other immune cells and localize at the site of microbial infection.^{8,9} Activated platelets release antibacterial substances, such as reactive oxygen species, antimicrobial peptides, defensins, and proteases, to kill bacterial pathogens.^{8,9} Platelet-related indicators, such

as platelet counts, platelet and leukocyte aggregates, and platelet-expressed selectin (P-selectin) levels, have been recognized as biomarkers to predict sepsis prognosis.^{5,10,11}

Neutrophil activation can induce the formation of neutrophil extracellular traps (NETs) to capture and phagocytose microbes in infected tissues.¹² Platelets are recruited to NETs and further promote the NET formation, enhancing the killing effect on the pathogens.¹³ During inflammation, platelets can be activated by pathogens or inflammatory factors and interact with neutrophils via P-selectin, CD40 L, Toll-like receptor4 (TLR4), and glycoprotein Ib α (GPIb α). This leads to NETosis and septic thrombosis.^{14–17} Excessive formation of NETs is an important cause of inflammatory thrombosis.¹⁸

Stimulator of interferon genes (STING) is an endoplasmic reticulum junction and sensing protein, which is important for inflammatory responses to pathogen-associated molecular pattern molecules (PAMPs) during infection.¹⁹ STING can be activated by small nucleotides, such as cyclic dinucleotides (CDNs), to induce the innate immune responses.²⁰ Cyclic guanosine monophosphate adenosine monophosphate (cGAMP), a common

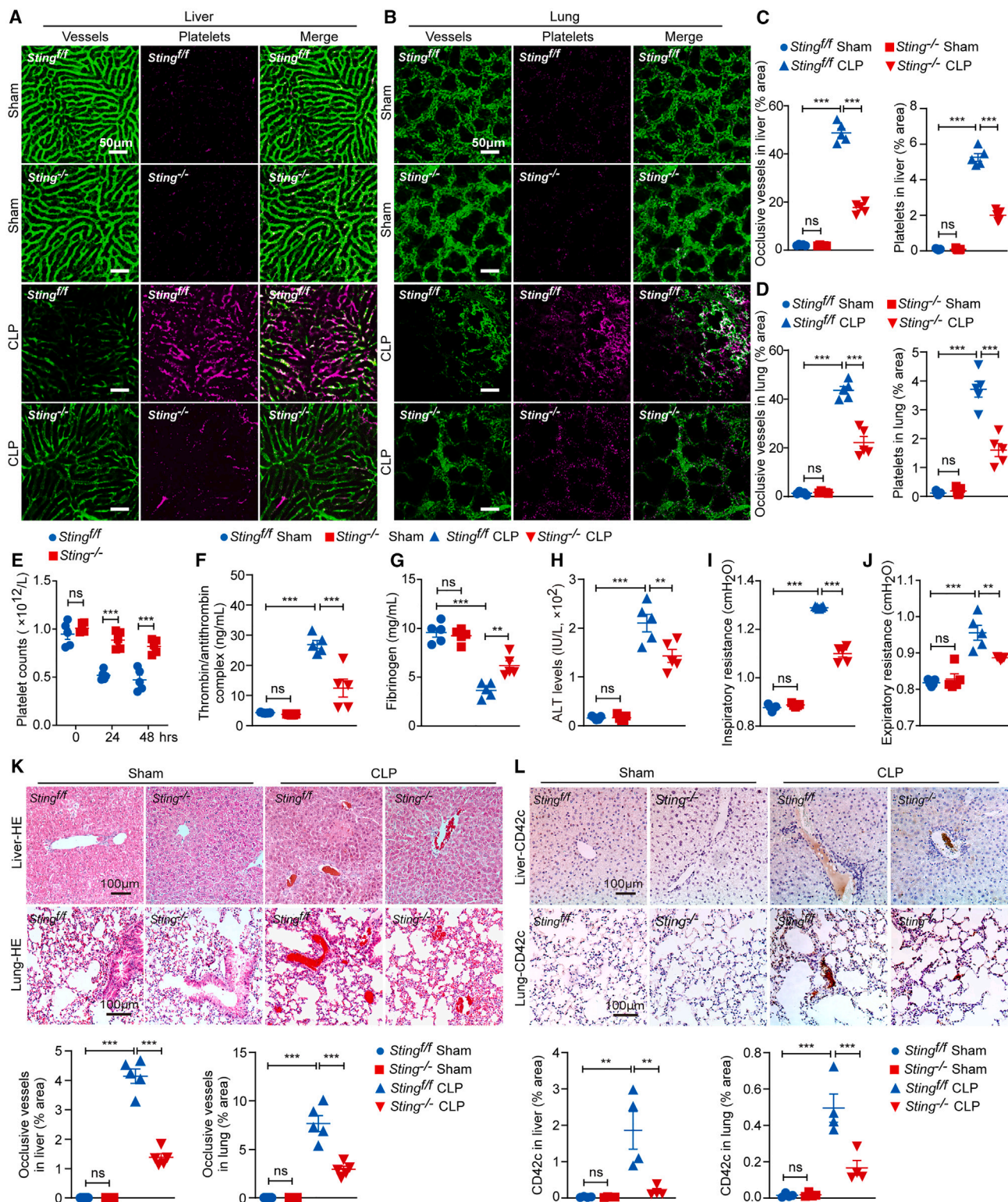


Figure 1. Platelet STING deficiency alleviates sepsis-induced thrombosis

(A) Representative intravital microscopy (IVM) images of blood flow (FITC-dextran 2000, green) and platelets (DyLight649-GP1b β , deep red) in the liver vasculatures of sham and CLP-operated *Sting*^{fl/fl} and *Sting*^{-/-} mice. Scale bars: 50 μ m.

(B) Representative multiphoton microscopy images of blood flow (FITC-dextran 2000, green) and platelets (DyLight649-GP1b β , deep red) in the lung vasculatures of sham and CLP-operated *Sting*^{fl/fl} and *Sting*^{-/-} mice. Scale bars: 50 μ m.

(legend continued on next page)

agonist of STING, is produced in mammalian cells by cGAMP synthase (cGAS) in response to cytoplasmic DNA or by exogenous microbial infection.²¹ STING activation induces the expression of type I interferon (IFN) and other inflammatory factors through the TANK-binding kinase 1 (TBK1)/IFN regulatory factor 3 (IRF3) and the NF- κ B signaling pathway.²² Platelets are important cells in the thrombus formation and are critical for inflammation.²³ However, it is unknown whether STING regulates platelet function during inflammatory thrombosis.

In this study, we found that platelet STING exacerbated sepsis-induced thrombosis by promoting platelet activation and NETosis. Mechanistically, STING interacted with syntaxin binding protein 2 (STXBP2) to maintain the soluble N-ethylmaleimide-sensitive fusion protein (NSF) attachment protein receptor (SNARE) complex assembly and further granule secretion in platelets. Moreover, sepsis-derived cGAMP could facilitate the SNARE complex assembly and accelerate platelet granule release and septic thrombosis, which probably depends on the palmitoylation of STING. These findings reveal that STING is a potential target for the treatment of platelet-related septic thrombosis.

RESULTS

Platelet STING deficiency alleviates sepsis-induced thrombosis

The occurrence of sepsis leads to platelet activation and the increased risk of thrombosis.³ To explore the role of platelet STING in sepsis-induced thrombosis, platelet STING-deficient mice (*Sting*^{fl/fl} *Pf4-Cre*⁺, *Sting*^{-/-}) and control mice (*Sting*^{fl/fl} *Pf4-Cre*⁻, *Sting*^{fl/fl}) were generated (Figure S1A). The protein levels of STING were decreased in *Sting*^{-/-} platelets but remained unchanged in other hemocytes (Figure S1B). *Sting*^{-/-} mice did not show changes in the numbers or proportions of hemocytes in the peripheral blood compared with those of *Sting*^{fl/fl} mice (Figure S1C–S1I).

Cecal ligation and puncture (CLP), a classic polymicrobial sepsis model, can mimic the progression and complications of human sepsis, including the occurrence of thrombosis and NETosis.^{24,25} *Sting*^{fl/fl} and *Sting*^{-/-} mice were subjected to CLP-induced sepsis, and the dynamic process of septic thrombosis within the vessels of the mouse livers and lungs was visualized by intravital microscopy. In the CLP-operated group, there was occlusion in the vessels of the livers and lungs, as platelets were aggregated in the vessels of *Sting*^{fl/fl} mice (Figures 1A–1D; Videos S1 and S2). Platelet STING deficiency attenuated platelet aggregation and vascular thrombosis (Figures 1A–1D; Videos S1 and S2). In addition, platelet transfusion experiments were performed to further confirm the role of platelet STING in septic thrombosis. *Sting*^{fl/fl} and *Sting*^{-/-} platelets were separately trans-

fused into sham and CLP-operated wild-type (*WT*) mice. CLP-*WT* mice transfused with *Sting*^{-/-} platelets had reduced thrombus formation compared with that transfused with *Sting*^{fl/fl} platelets, suggesting the regulatory function of platelet STING in septic thrombosis (Figures S2A and S2B).

DIC indicators, such as platelet counts, plasma thrombin/antithrombin (TAT), and fibrinogen, were also measured. CLP-*Sting*^{-/-} mice had increased platelet counts and fibrinogen levels and decreased TAT complex levels (Figures 1E–1G), demonstrating that platelet STING deficiency could protect CLP-mice from the risk of excessive septic thrombosis. Moreover, CLP-*Sting*^{-/-} mice had less damage in the livers and lungs than CLP-*Sting*^{fl/fl} mice (Figures 1H–1J), indicating that STING deletion in platelets could protect mice from liver and lung damage in sepsis.

The pathological structures of the liver and lung tissues in sham and CLP *Sting*^{fl/fl} and *Sting*^{-/-} mice were also analyzed using histopathologic examination (HE) and immunohistochemical (IHC). There was a massive accumulation of platelets and thrombi in the vessels of the livers and lungs in CLP-*Sting*^{fl/fl} mice (Figures 1K and 1L). By contrast, platelet aggregation and thrombus occlusion were inhibited in CLP-*Sting*^{-/-} mice, echoing the findings of *in vivo* intravital microscopy (Figures 1K and 1L). These findings suggest that platelet STING plays a critical role in sepsis-induced thrombosis.

Platelet STING deficiency suppresses NET formation in sepsis

To explore the role of platelet STING in the pathogenesis of sepsis, the survival rate of CLP-*Sting*^{fl/fl} and *Sting*^{-/-} mice was monitored for up to 7 days. The survival rate of *Sting*^{-/-} mice was higher than that of *Sting*^{fl/fl} mice after surgery (Figure 2A). The development of sepsis is accompanied by the release of platelet granules and the aggregation of platelets and other immunocytes.²⁶ We found that STING deficiency suppressed P-selectin expression, neutrophil/monocyte-platelet aggregation, and JON/A binding in the CLP model at the indicated time points after surgery (Figures 2B–2D and S2C).

Platelets are believed to be involved in the formation of NETs during the development of sepsis.²⁷ To further investigate the role of platelet STING in the formation of NETs, the levels of the myeloperoxidase (MPO)-DNA complex were examined, and the results showed that the NET production was reduced in CLP-operated *Sting*^{-/-} mice (Figure 2E). NETosis was also visualized by intravital microscopy, and the numbers of NET-forming neutrophils were quantified. The corresponding images and statistical results demonstrated that platelet STING deficiency inhibited the formation of NETs and thrombi in the livers and lungs during sepsis (Figures 2F, 2G, and S2D).

(C and D) Quantitative analysis of the ratio of occlusive vessels and platelets in livers and lungs of sham and CLP-operated *Sting*^{fl/fl} and *Sting*^{-/-} mice (n=5).

(E) Platelet counts in the peripheral blood of *Sting*^{fl/fl} and *Sting*^{-/-} mice after CLP surgery at indicated time points (n = 5).

(F and G) Plasma thrombin/antithrombin complex (TAT) and fibrinogen levels of sham and CLP-operated *Sting*^{fl/fl} and *Sting*^{-/-} mice (n = 5).

(H) Plasma alanine aminotransferase (ALT) levels of sham and CLP-operated *Sting*^{fl/fl} and *Sting*^{-/-} mice (n = 5).

(I and J) Inspiratory resistance and expiratory resistance of sham and CLP-operated *Sting*^{fl/fl} and *Sting*^{-/-} mice (n = 5).

(K and L) HE staining and IHC staining of CD42c in livers and lungs of *Sting*^{fl/fl} and *Sting*^{-/-} mice in the sham and CLP groups. HE staining statistical analysis for thrombus area in *Sting*^{fl/fl} and *Sting*^{-/-} mice livers and lungs was shown (n = 5). IHC staining statistical analysis for positive thrombus area in *Sting*^{fl/fl} and *Sting*^{-/-} mice livers and lungs is shown (n = 4). Scale bars: 100 μ m.

Data are shown as the mean \pm SEM from three independent experiments. **p < 0.01; ***p < 0.001; ns, no significance (one-way and two-way ANOVA test).

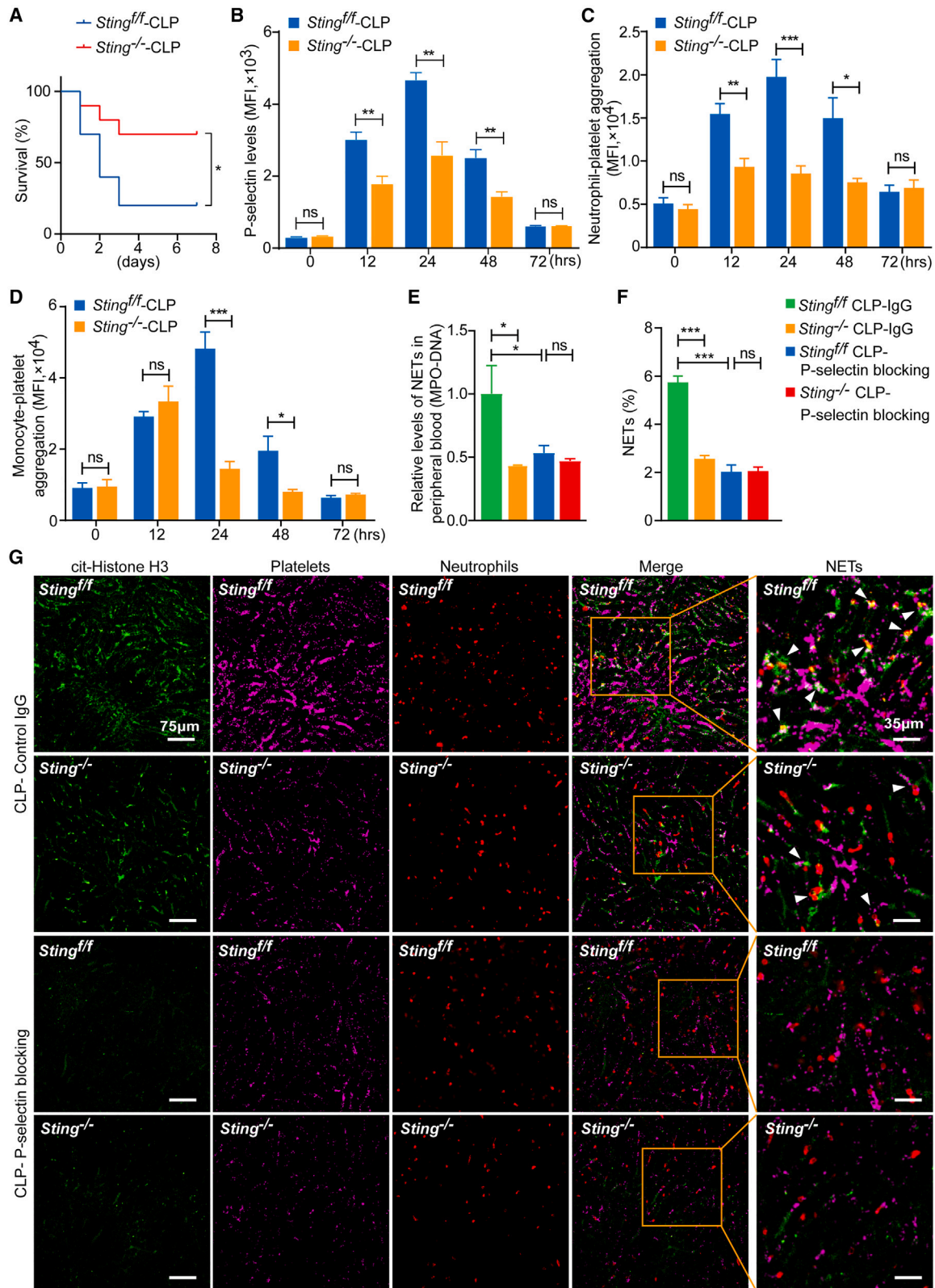


Figure 2. Platelet STING deficiency suppresses NET formation in sepsis

(A) Survival curves of *Sting^{fl/fl}* and *Sting^{-/-}* mice after the CLP surgery in sepsis (n = 10, Kaplan-Meier survival analysis).

(B) The levels of P-selectin exposure in *Sting^{fl/fl}* and *Sting^{-/-}* platelets at indicated time points after CLP (n = 5).

(legend continued on next page)

The interaction of P-selectin and PSGL1 mediates neutrophil-platelet aggregation and NETosis.¹⁵ To further explore the role of STING in P-selectin exposure during NETosis, P-selectin blocking antibodies were administered to CLP-operated *Sting*^{fl/fl} and *Sting*^{-/-} mice. Blocking P-selectin inhibited the formation of NETs and the interaction of platelets and neutrophils in CLP-*Sting*^{fl/fl} mice to comparable levels of that in CLP-*Sting*^{-/-} mice (Figures 2E–2G and S3A). These results suggested that P-selectin played an essential role in the progression of STING-mediated NETosis during sepsis. In addition, blocking P-selectin suppressed plasma P-selectin levels in CLP-*Sting*^{fl/fl} mice but had no effect on the surface CD40L levels in platelets or soluble CD40L (sCD40L) levels in the plasma (Figures S3B–S3D).

The role of integrin α IIb β 3 in platelet STING-mediated septic thrombosis was also assessed by treating CLP-operated *Sting*^{fl/fl} and *Sting*^{-/-} mice with tirofiban, a classical antagonist of α IIb β 3. Tirofiban could suppress JON/A levels in both *Sting*^{fl/fl} and *Sting*^{-/-} platelets *in vitro* (Figure S3H) and inhibit CLP-induced thrombosis *in vivo* (Figures S3E–S3G), suggesting that integrin α IIb β 3 activation also plays an important role in sepsis-induced thrombosis.

cGAMP facilitates platelet activation in a STING-dependent manner

Severe sepsis is associated with the activation of coagulation and immune systems.²⁸ To identify the driver of platelet activation in sepsis, septic plasma was incubated with *Sting*^{fl/fl} and *Sting*^{-/-} platelets. Septic plasma facilitated P-selectin exposure to a higher extent in *Sting*^{fl/fl} platelets than that in *Sting*^{-/-} platelets (Figure 3A). Moreover, the levels of cGAMP, the direct activator of STING, were increased in the plasma and platelets of CLP-operated mice (Figures 3B and S4A). To investigate whether cGAMP is the agonist of STING-mediated platelet activation, *Sting*^{fl/fl} and *Sting*^{-/-} platelets (as well as human platelets) were incubated with cGAMP, and their activation levels were measured. Compared with the controls, cGAMP treatment could facilitate platelet aggregation, P-selectin exposure, JON/A binding, spreading ability, and clot retraction in a STING-dependent manner, leading to platelet hyperactivation (Figures 3C–3E, S4B–S4G, and S5A–S5C).

Posttranslational modifications of STING were then assayed. There was no ubiquitination, phosphorylation, or SUMOylation (small ubiquitin-like modifier [SUMO]) of STING in human and septic mouse platelets *in vitro* or *in vivo* (Figures S5D and S5E). However, STING could be palmitoylated in platelets stimulated by cGAMP and thrombin, as well as platelets from CLP-operated mice (Figures 3F and S5F). Septic plasma treatment also induced palmitoylation of STING in platelets (Figure S5G). To further elucidate the role of STING palmitoylation in cGAMP-promoted platelet activation, H151, an inhibitor of STING palmitoy-

lation, was used. H-151 eliminated the hyperactivation levels of platelets treated with cGAMP in response to thrombin, indicating that the palmitoylation of STING promoted platelet activation in septic thrombosis (Figures 3G, 3H, and S5H).

The results above indicated that platelet STING could facilitate the activation of platelets during sepsis. We noticed that STING deficiency partially suppressed platelet responses to thrombin and collagen under physiological conditions, as evidenced by the lower levels of aggregation, granule secretion, and integrin activation in *Sting*^{-/-} platelets than controls (Figures 3C–3E and S5A–S5C). However, there was no difference in tail bleeding time, venous thrombosis in the inferior vena cava stenosis model, or platelet turnover between *Sting*^{fl/fl} and *Sting*^{-/-} mice (Figures S6A–S6C), except for slightly prolonged occlusion time in FeCl₃-induced carotid artery thrombosis *in vivo* in *Sting*^{-/-} mice (Figure S6D). There was also no cGAMP formed during the physiological platelet activation (data not shown). Moreover, the STING/TBK1/IRF3 signaling pathway was not activated in platelets treated with cGAMP and thrombin (Figure S6E), implying new mechanisms by which STING regulates platelet activation under physiological and pathological conditions.

STING promotes platelet granule secretion

Granule secretion plays an important role in platelet activation, thrombosis, and NETosis during sepsis.^{8,26} The release of platelet granules can be detected by their respective markers. Platelet STING deficiency suppressed the release of various granules (Figures 4A–4C), suggesting that STING regulated platelet granule secretion. Furthermore, cGAMP could facilitate the secretion of respective granules, consistent with the promoting effect of cGAMP on platelet activation. In addition, the numbers and substructures of *Sting*^{-/-} platelet granules were not altered compared with those of *Sting*^{fl/fl} platelets (Figure 4D), demonstrating that STING deletion did not affect platelet granule numbers but inhibited the process of platelet granule secretion. Moreover, STING was found to be partially located in platelet granules, further suggesting that STING had a regulatory effect on granule secretion (Figure 4E).

STING-interacting proteins were identified through immunoprecipitation (IP) and mass spectrometry in resting platelets. The Gene Ontology (GO) and Kyoto Encyclopedia of Genes and Genomes (KEGG) pathways associated with these identified proteins were further analyzed. STING-interacting proteins were closely associated with vesicle-mediated transport in platelets (Figure 4F). The KEGG pathways further indicated that STING participated in the SNARE-mediated vesicle transport (Figure 4G).

These results demonstrate that platelet STING deficiency impairs the platelet granule secretion and cGAMP further promotes the platelet granule secretion in response to thrombin, which may be caused by the involvement of STING in vesicle-mediated transport.

(C and D) The neutrophil-platelet aggregation and monocyte-platelet aggregation levels at indicated time points after surgery of *Sting*^{fl/fl} and *Sting*^{-/-} mice (n = 5). (E) Quantitative analysis of NETs within the liver of CLP-operated *Sting*^{fl/fl} and *Sting*^{-/-} mice treated with IgG or anti-CD62P antibodies by MPO-DNA ELISA (n = 5). (F) The quantify of NET-forming neutrophils in per random field of view (n = 5). (G) Representative of IVM images of NETs in the livers of *Sting*^{fl/fl} and *Sting*^{-/-} mice treated with IgG or anti-CD62P antibodies in CLP groups. Neutrophils were observed in red (Alexa Fluor 594-Ly-6G), NETs were observed in green (Alexa Fluor 488-cit-histone H3), and platelets were observed in dark red (DyLight649-GP1b β). Scale bars: 75 μ m.

Data are shown as the mean \pm SEM from three independent experiments. *p < 0.05; **p < 0.01; ***p < 0.001; ns, no significance (Kaplan-Meier survival analysis, unpaired t test and one-way ANOVA test).

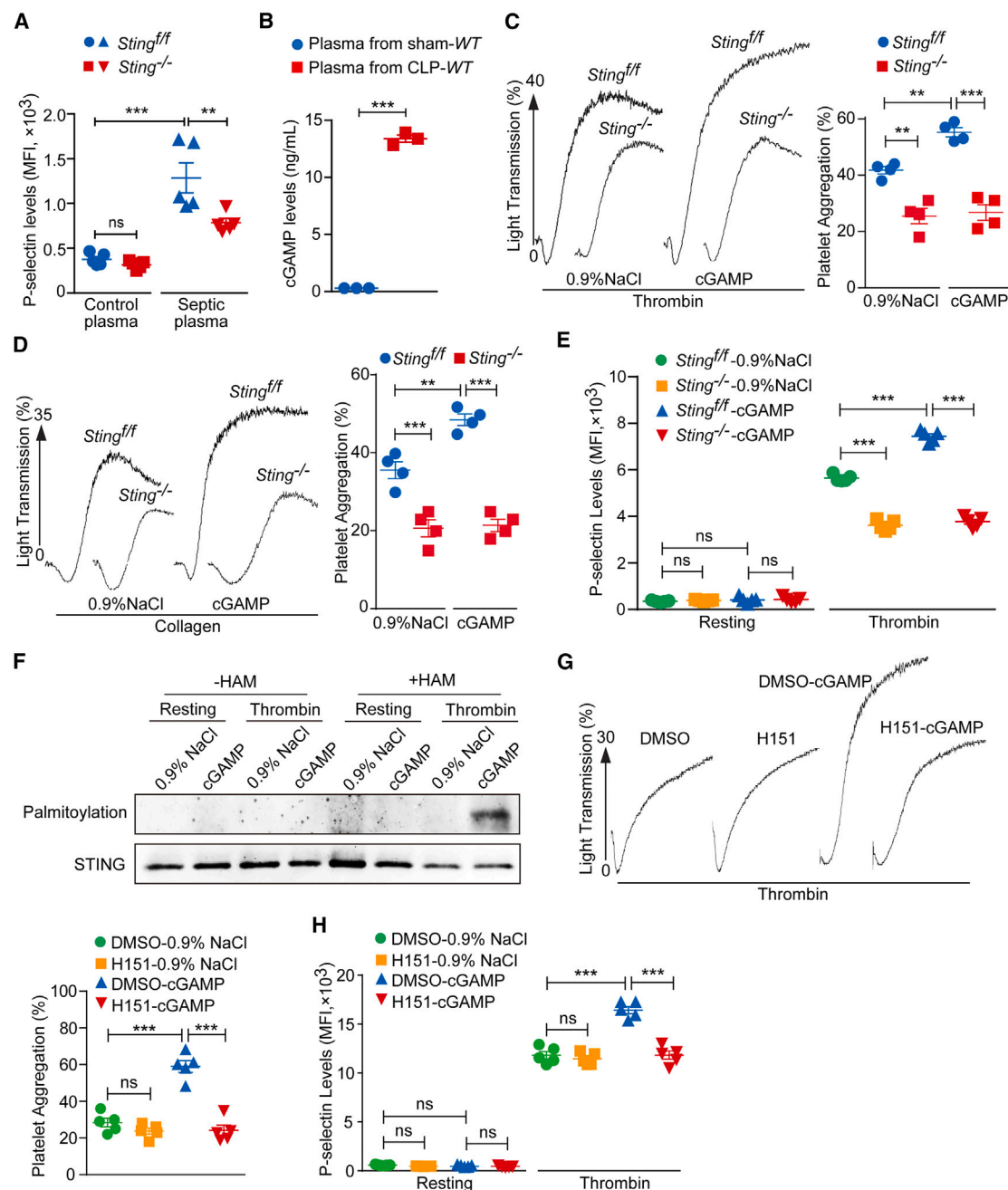


Figure 3. cGAMP facilitates platelet activation in a STING-dependent manner

(A) P-selectin exposure levels of *Sting*^{+/+} and *Sting*^{-/-} platelets incubated with plasma from sham or CLP-operated *WT* mice (n = 5). (B) cGAMP levels in the plasma of sham and CLP-operated *WT* mice (n = 3). (C and D) Aggregation of platelets from *Sting*^{+/+} and *Sting*^{-/-} mice treated with 0.9% NaCl or cGAMP in response to thrombin or collagen (n = 4). (E) P-selectin expression of *Sting*^{+/+} and *Sting*^{-/-} platelets treated with 0.9% NaCl or cGAMP in response to thrombin (n = 5). (F) The level of STING palmitoylation in human platelets treated with or without thrombin or cGAMP using acyl-biotin exchange (ABE). (G) Aggregation of human platelets treated with or without H151 in response to thrombin and cGAMP (n = 5). (H) Flow cytometric analysis of P-selectin exposure of human platelets treated with or without H151 and cGAMP in response to thrombin (n = 5). Data are shown as the mean ± SEM from three independent experiments. **p < 0.01; ***p < 0.001; ns, no significance (unpaired t test and one-way ANOVA test).

STING regulates the SNARE complex assembly by associating with STXBP2

By investigating STING-interacting proteins, we identified STXBP2, an important regulatory protein of the SNARE complex

(Figure S7A). Exogenous overexpressed and endogenous STING were found to interact with STXBP2, respectively (Figures 5A and 5C). Immunofluorescence results further demonstrated that STING colocalized with STXBP2 in spreading platelets

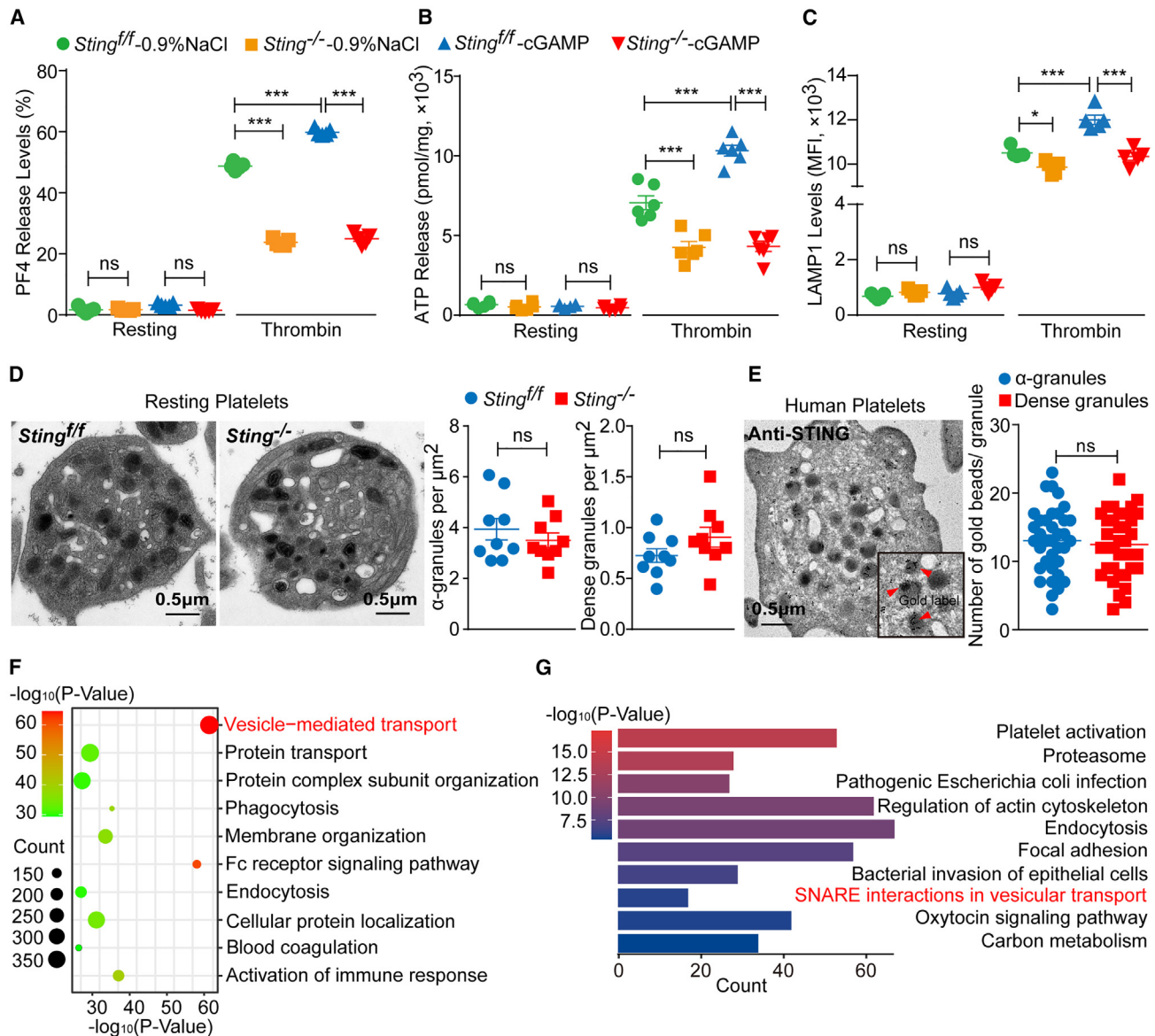


Figure 4. STING promotes platelet granule secretion

(A and B) PF4 levels (n = 5) and ATP levels (n = 6) in the supernatant of *Sting*^{fl/fl} and *Sting*^{-/-} platelets treated with 0.9% NaCl or cGAMP in response to thrombin. (C) Flow cytometric analysis of LAMP1 in *Sting*^{fl/fl} and *Sting*^{-/-} platelets treated with 0.9% NaCl or cGAMP in response to thrombin (n = 5). (D) Representative TEM images of *Sting*^{fl/fl} and *Sting*^{-/-} platelets. Platelet granule numbers were quantified using per unit area of counted granules (n = 9). Scale bars: 0.5 μm. (E) Representative immunoelectron microscopy (IEM) image for presenting the location of STING in platelet granules. Quantitative analysis of the numbers of gold beads in different platelet granules (n = 36). Scale bars: 0.5 μm. (F and G) GO pathway and KEGG pathway were enriched by the database for annotation, visualization, and integrated discovery (DAVID) from tandem mass spectrometry data (the identified interaction proteins of STING in resting platelets). Data are shown as the mean ± SEM from three independent experiments. *p < 0.05; ***p < 0.001; ns, no significance (unpaired t test and one-way ANOVA test).

(Figure S7B). The SNARE complex assembly is involved in platelet granule secretion.²⁹ To explore the role of STING in the SNARE complex assembly, platelets from *Sting*^{fl/fl} and *Sting*^{-/-} mice were prepared and subjected to IP. STING deletion in platelets suppressed the SNARE complex assembly, as there were lower binding levels of syntaxin11, vesicle-associated membrane protein 8 (VAMP8), and synaptosome-associated protein 23 (SNAP23) to STXBP2. In addition, STING deficiency did not affect

the protein expression levels of the key SNARE complex components (Figure 5B).

Our results also showed that cGAMP could facilitate platelet granule release in response to thrombin (Figures 4A–4C), suggesting that cGAMP may affect the SNARE complex assembly. The stimulation of cGAMP and thrombin promoted the interaction between STING and STXBP2 and the assembly of the SNARE complex in platelets (Figures 5C and 5D). Furthermore, H151 could

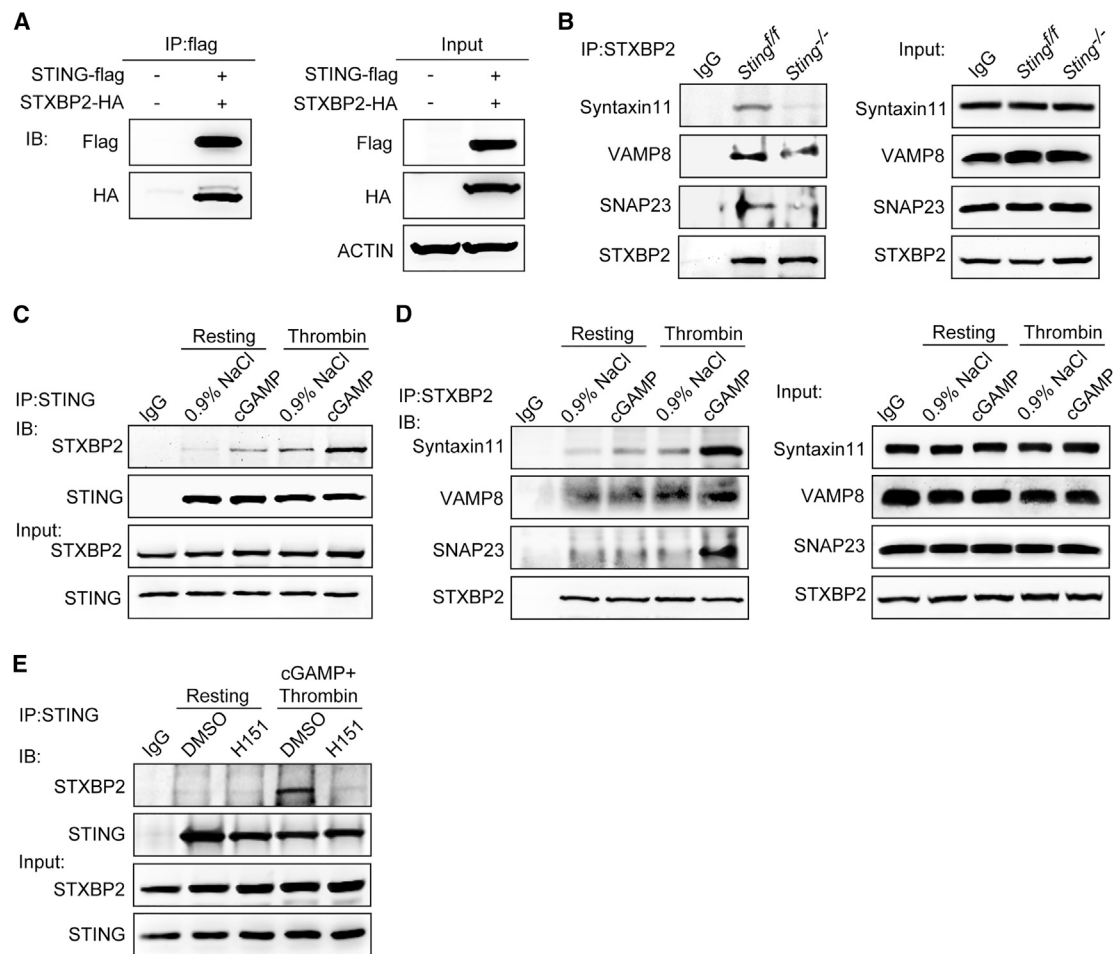


Figure 5. STING regulates the SNARE complex assembly by associating with STXBP2

(A) IP-FLAG assay of the lysates of HEK293T cells transfected with STING-FLAG and STXBP2-HA.

(B) IP-STXBP2 assay of the lysates of platelets from *Sting^{fl/fl}* and *Sting^{-/-}* mice. The SNARE complex protein expression in platelets was tested using anti-Syntaxin11, anti-VAMP8, and anti-SNAP23 antibodies.

(C) IP-STING assay of human platelets treated with or without thrombin or cGAMP. Isotype-matched IgG served as the negative control.

(D) IP-STXBP2 assay of human platelets treated with or without thrombin or cGAMP. Isotype-matched IgG served as the negative control.

(E) IP-STING assay of human platelets treated with or without H151 in response to thrombin and cGAMP. Isotype-matched IgG served as the negative control.

suppress the promoting effect of STING binding to STXBP2 in platelets stimulated by thrombin and cGAMP (Figure 5E), which was consistent with the results of H151 eliminating platelet hyperactivation induced by cGAMP and thrombin (Figures 3G and 3H).

These results suggest that platelet STING is involved in the SNARE complex assembly and granule release under physiological conditions. cGAMP promotes the binding of STING to STXBP2 and the assembly of the SNARE complex, leading to platelet hyperactivation, which probably depends on the palmitoylation of STING.

The peptide ST5 suppresses the binding of STING to STXBP2 and platelet activation

STING contains transmembrane (TM) regions (amino-acid residues 1–139), a c-di-GMP binding domain (CBD, amino-acid residues 139–340) and a C-terminal tail (CTT, amino-acid residues 340–379).³⁰ IP results showed that STING could combine with

STXBP2 through the C-terminal domain (CTD, amino-acid residues 139–379) (Figure 6A). To explore the specific binding region of STING and STXBP2, the sequence of CTD was divided into 12 segments and the corresponding peptides were synthesized (Figure S7C). The results of the ELISA assay and protein-protein docking simulation indicated that ST5 was likely the optimal spatial region for STING binding to STXBP2 (Figures 6B and 6C). In addition, the ST5 peptide suppressed the binding levels of STING to STXBP2 (Figure 6D).

The peptide TAT (GRKKRRQRRR) from HIV is a kind of cell-penetrating peptide (CPP) that can help macromolecules cross the cell membrane through endocytosis.³¹ To substantiate the biological function of the ST5 peptide, ST5 with N-terminal TAT (C-ST5) was synthesized. The immunofluorescence results showed that C-ST5 could enter the cells (Figure S7D). Moreover, we found that the levels of aggregation and P-selectin exposure were decreased in C-ST5-treated platelets, compared with

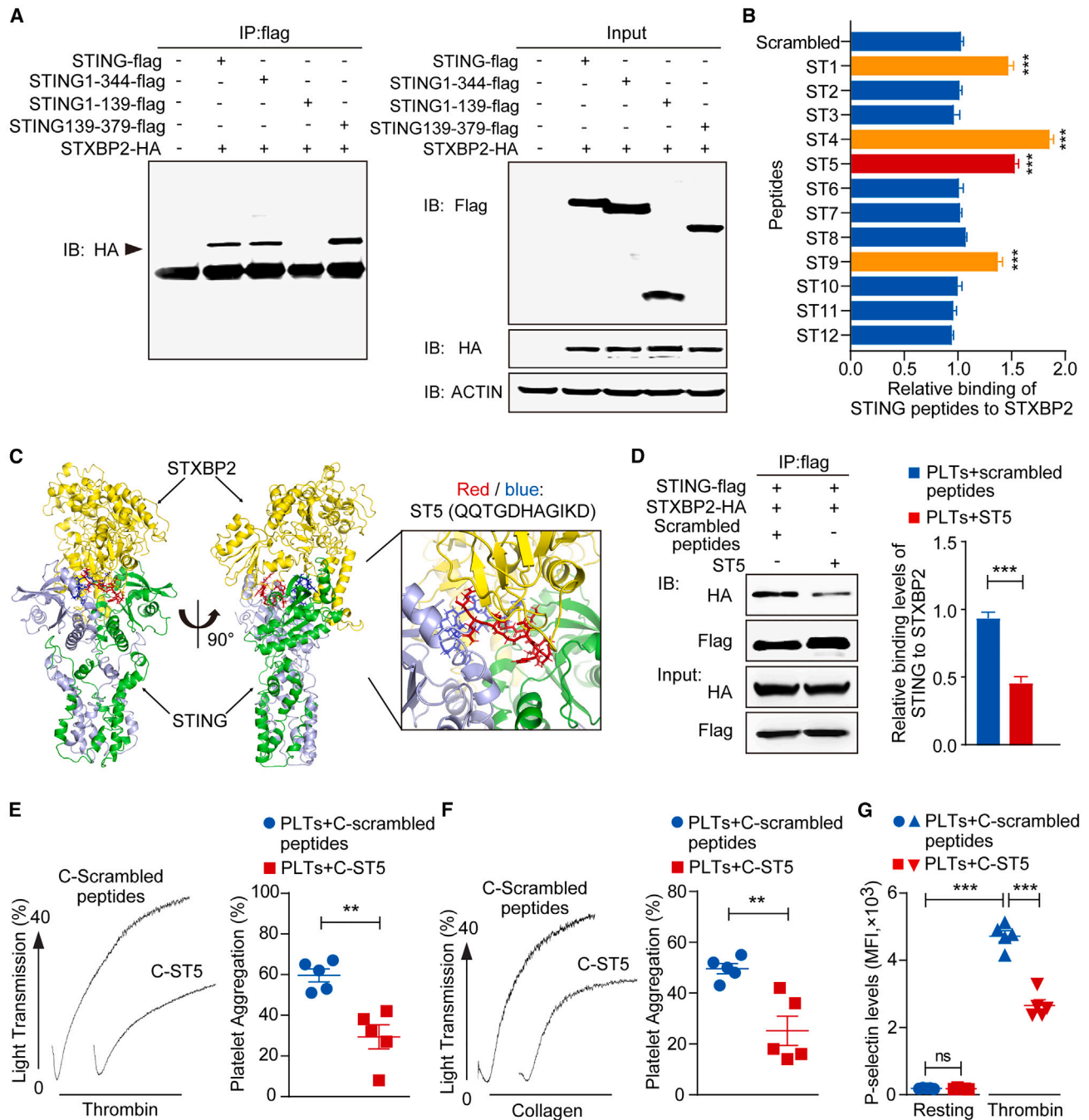


Figure 6. The peptide ST5 suppresses the binding of STING to STXBP2 and platelet activation

(A) IP-FLAG assay of the lysates of HEK293T cells transfected with STING-FLAG, STING 1–344-FLAG, STING 1–139-FLAG or STING 139–379-FLAG, and STXBP2-HA, respectively.

(B) Relative binding levels of peptide ST1–12 to STXBP2 by ELISA (n = 5).

(C) The binding model of STING to STXBP2.

(D) IP-FLAG assay of HEK293T cell lysates transfected with STING-FLAG and STXBP2-HA and treated with scrambled or ST5 peptides. Quantitative analysis of the gray values of STXBP2-HA bands (n = 5).

(E and F) Aggregation of human platelets treated with C-scrambled or C-ST5 peptides in response to thrombin and collagen (n = 5).

(G) The levels of P-selectin exposure in human platelets incubated with C-scrambled or C-ST5 peptides (n = 5).

Data are shown as the mean ± SEM from three independent experiments. **p < 0.01; ***p < 0.001; ns, no significance (unpaired t test and one-way ANOVA test).

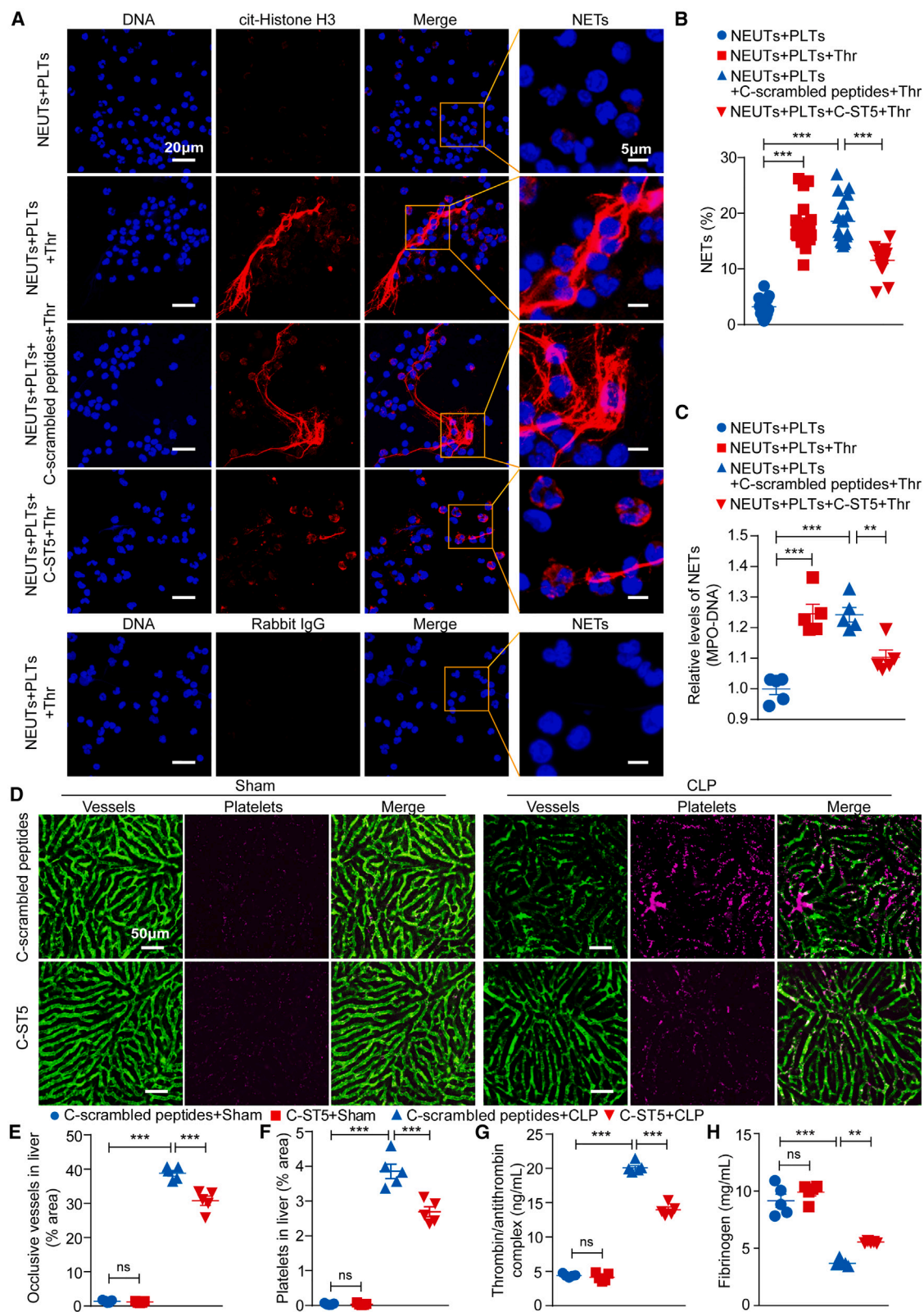


Figure 7. The peptide C-ST5 suppresses NETs formation and sepsis-induced thrombosis

(A) Representative immunofluorescence images of NETs *in vitro* (isolated human neutrophils cultured with platelets in the presence of C-scrambled or C-ST5 peptides): DNA (blue) and cit-histone H3 (red). Scale bars: 20 μ m.

(legend continued on next page)

scrambled peptide-treated platelets (Figures 6E–6G). Together, these results suggest that C-ST5 inhibits platelet activation *in vitro*.

The peptide C-ST5 suppresses NET formation and sepsis-induced thrombosis

To further explore the function of the peptide C-ST5 on NETosis mediated by activated platelets, the formation of NETs was observed. Compared with the C-scrambled peptides, C-ST5 suppressed the production of NETs (Figures 7A and 7B). The MPO-DNA levels in the supernatant of C-ST5-treated platelets/neutrophils were also decreased compared with that treated with C-scrambled peptides (Figure 7C). These results suggest that C-ST5 inhibits platelet-mediated NET formation.

The CLP model was also performed to further investigate the function of C-ST5 on septic thrombosis *in vivo*. C-ST5 was found to suppress septic thrombosis in CLP mice (Figures 7D–7F). Additionally, CLP-WT mice treated with C-ST5 had lower levels of TAT complex and higher levels of fibrinogen, compared with those treated with the C-scrambled peptide (Figures 7G and 7H). These results suggest the potential intervention effect of C-ST5 on septic thrombosis.

DISCUSSION

Immune inflammatory thrombosis induced by pathogen infection is a major cause of multiorgan dysfunction and death.³² STING, as an important regulator of innate immunity, can effectively mediate immune inflammation in response to pathogen infection.³³ STING activation is probably correlated with hypercoagulability and poor outcomes in patients with SARS-CoV-2 infection.³⁴ Platelets, the key hemocytes of thrombosis, also perform innate immune defense against pathogen infection.³⁵ The expression of STING was detected in platelets; however, it is unknown whether STING regulates platelet functions and thrombus formation during pathogen infections. In our study, we demonstrated that STING played a critical role in platelet granule secretion, septic thrombosis, and NETosis. We also revealed a new mechanism by which platelet STING interacted with STXBP2 to regulate the assembly of the SNARE complex, which further affected platelet granule release, activation, and ultimately participated in the formation of septic thrombus.

STING plays a crucial role in the intracellular response to nucleic acids.²² After exogenous or endogenous DNA being recognized by cGAS, STING is activated and then recruits TBK1 to phosphorylate IRF3, which induces IRF3 entering the nucleus and then initiates the expression of type I IFN.³⁶ In addition to the traditionally recognized pathway, STING also plays a nonclassical role in ER stress-mediated Gasdermin D

(GSDMD) activation in macrophages and monocytes during coagulation.³⁷ In this study, we found that cGAMP could not trigger the activation of STING/TBK1/IRF3 signaling pathway but induced the palmitoylation of STING in thrombin-stimulated platelets, indicating a new regulatory mechanism of STING in septic thrombosis.

Granule-plasma membrane fusion is an important process in granule secretion, which regulates the physiological and pathological functions of platelets.^{38,39} The assembly of the SNARE complex, which contains syntaxin, VAMP, and SNAP-related proteins, regulates granule-plasma membrane fusion and vesicle trafficking.⁴⁰ STXBP2 has been identified as the chaperone of syntaxin11 and plays an essential role in the SNARE complex assembly in platelets.^{41,42} We found that STING interacted with STXBP2 through the CBD domain and thus regulated the SNARE complex assembly, granule secretion, and platelet activation. Moreover, cGAMP could further promote the binding of STING to STXBP2, platelet activation, and exacerbate septic thrombosis, which probably depends on the palmitoylation of STING.

The cGAS/STING pathway is involved in the activation of bacterial or viral infection-induced innate immunity.^{33,43} cGAMP, the agonist of STING, can be directly derived from bacterial pathogens.⁴⁴ cGAS, a cytosolic DNA receptor, catalyzes the formation of cGAMP, facilitating the activation of STING in the setting of pathogen infection or cell stress.^{45,46} As cGAMP-promoted platelet activation has been shown to be essential for septic thrombosis induced by bacterial infection, the role of the cGAS/STING pathway in more extensive pathological thrombosis should be further investigated, such as DNA virus infection. Moreover, as various STING small molecule agonists for tumor immunotherapy are currently in the stage of preclinical trials, thrombosis might be considered a possible side effect.

Sepsis-induced thrombosis is a challenge in clinical treatment.^{47,48} Most drugs for antithrombotic therapy of sepsis, such as aspirin and P2Y₁₂ inhibitors, aim to inhibit platelet activation.⁴⁹ Notably, exploring the role of platelets in the development of sepsis and searching for new antiplatelet drugs from this perspective may allow for more effective treatment of sepsis-induced thrombosis. In this study, the ST5 peptide was found to inhibit the binding of STING to STXBP2 and suppress platelet activation, NETosis, and septic thrombosis both *in vitro* and *in vivo*, suggesting a potential intervention effect in associated thrombotic diseases.

In conclusion, our study reveals an important role of STING in the regulation of platelet function and suggests that targeting the interaction between STING and STXBP2 may be the potential intervention for the treatment of septic thrombosis.

(B) The quantity of NETs-forming neutrophils in each field of view (n = 17).

(C) Quantitative analysis of NETs by MPO-DNA ELISA (n = 5).

(D) Representative images of IVM in the livers of sham and CLP-operated WT mice injected with C-scrambled or C-ST5 peptides. Scale bars: 50 μ m.

(E) Quantification analysis of the ratio of occlusive vessels in the livers (n = 5).

(F) Quantification analysis of the platelets in the livers (n = 5).

(G and H) ELISA quantification of plasma TAT and fibrinogen after tail intravenous injection of C-scrambled or C-ST5 peptides in sham and CLP-operated WT mice (n = 5).

Data are shown as the mean \pm SEM from three independent experiments. **p < 0.01; ***p < 0.001; ns, no significance (one-way ANOVA test).

STAR★METHODS

Detailed methods are provided in the online version of this paper and include the following:

- **KEY RESOURCES TABLE**
- **RESOURCE AVAILABILITY**
 - Lead contact
 - Materials availability
 - Data and code availability
- **EXPERIMENTAL MODEL AND SUBJECT DETAILS**
 - Mice
 - Sepsis Model: Cecal Ligation and Puncture (CLP) Assay
 - Hemostasis Model: Mouse Tail Bleeding Assay
 - Arterial Thrombosis Model: FeCl₃-induced Carotid Artery Injury Assay
 - Vein Thrombosis Model: Inferior Vena Cava (IVC) Stenosis Assay
- **METHOD DETAILS**
 - Preparation for Intravital Microscopy (IVM)
 - IVM and Image Analysis
 - Multiphoton Laser Scanning Confocal Intravital Microscopy
 - Biochemical Assays and Lung Function Assays
 - Measurement of Neutrophil-Platelet and Monocyte-Platelet Aggregation
 - Platelet Preparation, Aggregation, P-selectin Exposure, JON/A Binding, PAC1 Binding, Spreading, and Clot Retraction
 - Platelet Secretion Analysis
 - Transmission Electron Microscopy (TEM) and Immunoelectron Microscopy (IEM)
 - Protein-Protein Docking
 - ELISA
 - NETosis Experiment *In Vitro*
 - Acyl-Biotin Exchange (ABE) Palmitoylation Assay
 - Platelet Transfusion Assay
 - Platelet Lifespan Assay
 - Plasmid Construction and Plasmid Transfection
 - The Synthesis of Peptides
 - Immunoprecipitation (IP)
 - Immunofluorescence and Confocal Microscopy
- **QUANTIFICATION AND STATISTICAL ANALYSIS**

SUPPLEMENTAL INFORMATION

Supplemental information can be found online at <https://doi.org/10.1016/j.immuni.2023.02.015>.

ACKNOWLEDGMENTS

The authors thank Kevin Liu from Vanderbilt University for proofreading the article. This work is supported by grants from the National Natural Science Foundation of China (82170126, 82030004, 31830050, 82200131, and 81900138), National Key R&D Program of China (2021YFA0804900), “Chenguang Program” supported by Shanghai Education Development Foundation and Shanghai Municipal Education Commission (20CG21), Innovative research team of high-level local universities in Shanghai (SHSMU-ZDCX20211801), China National Postdoctoral Program for Innovative Talents (BX2021186), Core Facility of Basic Medical Sciences in Shanghai Jiao Tong University School of Medicine, the Imaging Core of Shanghai Institute of Immu-

nology, and Shanghai Frontiers Science Center of Cellular Homeostasis and Human Diseases.

AUTHOR CONTRIBUTIONS

Conceptualization, H.J., J.L., and Y.X.; methodology, M.Y., H.J., C.D., L.Z., N.D., and G.L.; software, F.Z.; validation, M.Y. and H.J.; formal analysis, M.Y. and Y.X.; investigation, M.Y., H.J., J.W., and L.D.; resources, J.L. and Y.X.; writing – original draft, M.Y., H.J., and Y.X.; writing – review & editing, J.L. and Y.X.; visualization, M.Y., H.J., and Y.X.; supervision, J.L. and Y.X.; project administration, J.L. and Y.X.; funding acquisition, H.J., J.L., and Y.X.

DECLARATION OF INTERESTS

The authors declare no competing interests.

Received: January 28, 2022

Revised: November 9, 2022

Accepted: February 22, 2023

Published: March 20, 2023

REFERENCES

1. Singer, M., Deutschman, C.S., Seymour, C.W., Shankar-Hari, M., Annane, D., Bauer, M., Bellomo, R., Bernard, G.R., Chiche, J.D., Cooper-Smith, C.M., et al. (2016). The third international consensus definitions for sepsis and septic shock (Sepsis-3). *JAMA* 315, 801–810. <https://doi.org/10.1001/jama.2016.0287>.
2. Gando, S., Shiraishi, A., Yamakawa, K., Ogura, H., Saitoh, D., Fujishima, S., Mayumi, T., Kushimoto, S., Abe, T., Shiino, Y., et al. (2019). Role of disseminated intravascular coagulation in severe sepsis. *Thromb. Res.* 178, 182–188. <https://doi.org/10.1016/j.thromres.2019.04.025>.
3. Levi, M., Schultz, M., and van der Poll, T. (2013). Sepsis and thrombosis. *Semin. Thromb. Hemost.* 39, 559–566. <https://doi.org/10.1055/s-0033-1343894>.
4. Angus, D.C., and van der Poll, T. (2013). Severe sepsis and septic shock. *N. Engl. J. Med.* 369, 840–851. <https://doi.org/10.1056/NEJMra1208623>.
5. Greco, E., Lupia, E., Bosco, O., Vizio, B., and Montrucchio, G. (2017). Platelets and multi-organ failure in sepsis. *Int. J. Mol. Sci.* 18. <https://doi.org/10.3390/ijms18102200>.
6. van der Meijden, P.E.J., and Heemskerk, J.W.M. (2019). Platelet biology and functions: new concepts and clinical perspectives. *Nat. Rev. Cardiol.* 16, 166–179. <https://doi.org/10.1038/s41569-018-0110-0>.
7. Morrell, C.N., Aggrey, A.A., Chapman, L.M., and Modjeski, K.L. (2014). Emerging roles for platelets as immune and inflammatory cells. *Blood* 123, 2759–2767. <https://doi.org/10.1182/blood-2013-11-462432>.
8. de Stoppelaar, S.F., van, van 't Veer, C., and van der Poll, T. (2014). The role of platelets in sepsis. *Thromb. Haemost.* 112, 666–677. <https://doi.org/10.1160/TH14-02-0126>.
9. Klinger, M.H., and Jelkmann, W. (2002). Role of blood platelets in infection and inflammation. *J. Interferon Cytokine Res.* 22, 913–922. <https://doi.org/10.1089/10799900260286623>.
10. Song, J., Hu, D., He, C., Wang, T., Liu, X., Ma, L., Lin, Z., and Chen, Z. (2013). Novel biomarkers for early prediction of sepsis-induced disseminated intravascular coagulation in a mouse cecal ligation and puncture model. *J. Inflamm. (Lond)* 10, 7. <https://doi.org/10.1186/1476-9255-10-7>.
11. Zhao, L., Zhao, L., Wang, Y.Y., Yang, F., Chen, Z., Yu, Q., Shi, H., Huang, S., Zhao, X., Xiu, L., et al. (2020). Platelets as a prognostic marker for sepsis: A cohort study from the MIMIC-III database. *Med. (Baltim)* 99, e23151. <https://doi.org/10.1097/MD.00000000000023151>.
12. Brinkmann, V., Reichard, U., Goosmann, C., Fauler, B., Uhlemann, Y., Weiss, D.S., Weinrauch, Y., and Zychlinsky, A. (2004). Neutrophil extracellular traps kill bacteria. *Science* 303, 1532–1535. <https://doi.org/10.1126/science.1092385>.
13. McDonald, B., Urrutia, R., Yipp, B.G., Jenne, C.N., and Kubers, P. (2012). Intravascular neutrophil extracellular traps capture bacteria from the

- bloodstream during sepsis. *Cell Host Microbe* 12, 324–333. <https://doi.org/10.1016/j.chom.2012.06.011>.
14. Clark, S.R., Ma, A.C., Tavener, S.A., McDonald, B., Goodarzi, Z., Kelly, M.M., Patel, K.D., Chakrabarti, S., McAvoey, E., Sinclair, G.D., et al. (2007). Platelet TLR4 activates neutrophil extracellular traps to ensnare bacteria in septic blood. *Nat. Med.* 13, 463–469. <https://doi.org/10.1038/nm1565>.
 15. Etulain, J., Martinod, K., Wong, S.L., Cifuni, S.M., Schattner, M., and Wagner, D.D. (2015). P-selectin promotes neutrophil extracellular trap formation in mice. *Blood* 126, 242–246. <https://doi.org/10.1182/blood-2015-01-624023>.
 16. Rahman, M., Zhang, S., Chew, M., Ersson, A., Jeppsson, B., and Thorlacius, H. (2009). Platelet-derived CD40L (CD154) mediates neutrophil upregulation of Mac-1 and recruitment in septic lung injury. *Ann. Surg.* 250, 783–790. <https://doi.org/10.1097/SLA.0b013e3181bd95b7>.
 17. Simon, D.I., Chen, Z., Xu, H., Li, C.Q., Dong, Jf, McIntire, L.V., Ballantyne, C.M., Zhang, L., Furman, M.I., Berndt, M.C., and López, J.A. (2000). Platelet glycoprotein I α is a counterreceptor for the leukocyte integrin Mac-1 (CD11b/CD18). *J. Exp. Med.* 192, 193–204. <https://doi.org/10.1084/jem.192.2.193>.
 18. Fuchs, T.A., Brill, A., Duerschmied, D., Schatzberg, D., Monestier, M., Myers, D.D., Jr., Wroblewski, S.K., Wakefield, T.W., Hartwig, J.H., and Wagner, D.D. (2010). Extracellular DNA traps promote thrombosis. *Proc. Natl. Acad. Sci. USA* 107, 15880–15885. <https://doi.org/10.1073/pnas.1005743107>.
 19. Barber, G.N. (2015). STING: infection, inflammation and cancer. *Nat. Rev. Immunol.* 15, 760–770. <https://doi.org/10.1038/nri3921>.
 20. Cong, X., Yuan, Z., Du, Y., Wu, B., Lu, D., Wu, X., Zhang, Y., Li, F., Wei, B., Li, J., et al. (2019). Crystal structures of porcine STING(CBD)-CDN complexes reveal the mechanism of ligand recognition and discrimination of STING proteins. *J. Biol. Chem.* 294, 11420–11432. <https://doi.org/10.1074/jbc.RA119.007367>.
 21. Sun, L., Wu, J., Du, F., Chen, X., and Chen, Z.J. (2013). Cyclic GMP-AMP synthase is a cytosolic DNA sensor that activates the type I interferon pathway. *Science* 339, 786–791. <https://doi.org/10.1126/science.1232458>.
 22. Burdette, D.L., Monroe, K.M., Sotelo-Troha, K., Iwig, J.S., Eckert, B., Hyodo, M., Hayakawa, Y., and Vance, R.E. (2011). STING is a direct innate immune sensor of cyclic di-GMP. *Nature* 478, 515–518. <https://doi.org/10.1038/nature10429>.
 23. Vieira-de-Abreu, A., Campbell, R.A., Weyrich, A.S., and Zimmerman, G.A. (2012). Platelets: versatile effector cells in hemostasis, inflammation, and the immune continuum. *Semin. Immunopathol.* 34, 5–30. <https://doi.org/10.1007/s00281-011-0286-4>.
 24. Czaikoski, P.G., Mota, J.M., Nascimento, D.C., Sônego, F., Castanheira, F.V., Melo, P.H., Scortegagna, G.T., Silva, R.L., Barroso-Sousa, R., Souto, F.O., et al. (2016). Neutrophil extracellular traps induce organ damage during experimental and clinical sepsis. *PLoS One* 11, e0148142. <https://doi.org/10.1371/journal.pone.0148142>.
 25. Rittirsch, D., Huber-Lang, M.S., Flierl, M.A., and Ward, P.A. (2009). Immunodesign of experimental sepsis by cecal ligation and puncture. *Nat. Protoc.* 4, 31–36. <https://doi.org/10.1038/nprot.2008.214>.
 26. Manne, B.K., Xiang, S.C., and Rondina, M.T. (2017). Platelet secretion in inflammatory and infectious diseases. *Platelets* 28, 155–164. <https://doi.org/10.1080/09537104.2016.1240766>.
 27. Caudrillier, A., Kessenbrock, K., Gilliss, B.M., Nguyen, J.X., Marques, M.B., Monestier, M., Toy, P., Werb, Z., and Looney, M.R. (2012). Platelets induce neutrophil extracellular traps in transfusion-related acute lung injury. *J. Clin. Invest.* 122, 2661–2671. <https://doi.org/10.1172/JCI61303>.
 28. van der Poll, T., and Levi, M. (2012). Crosstalk between inflammation and coagulation: the lessons of sepsis. *Curr. Vasc. Pharmacol.* 10, 632–638. <https://doi.org/10.2174/157016112801784549>.
 29. Flaumenhaft, R. (2003). Molecular basis of platelet granule secretion. *Arterioscler. Thromb. Vasc. Biol.* 23, 1152–1160. <https://doi.org/10.1161/01.ATV.0000075965.88456.48>.
 30. Wu, S., Zhang, Q., Zhang, F., Meng, F., Liu, S., Zhou, R., Wu, Q., Li, X., Shen, L., Huang, J., et al. (2019). HER2 recruits AKT1 to disrupt STING signalling and suppress antiviral defence and antitumour immunity. *Nat. Cell Biol.* 21, 1027–1040. <https://doi.org/10.1038/s41556-019-0352-z>.
 31. Copolovici, D.M., Langel, K., Eriste, E., and Langel, Ü. (2014). Cell-penetrating peptides: design, synthesis, and applications. *ACS Nano* 8, 1972–1994. <https://doi.org/10.1021/nm4057269>.
 32. Semeraro, N., Ammollo, C.T., Semeraro, F., and Colucci, M. (2012). Sepsis, thrombosis and organ dysfunction. *Thromb. Res.* 129, 290–295. <https://doi.org/10.1016/j.thromres.2011.10.013>.
 33. Liu, N., Pang, X., Zhang, H., and Ji, P. (2021). The cGAS-STING pathway in bacterial infection and bacterial immunity. *Front. Immunol.* 12, 814709. <https://doi.org/10.3389/fimmu.2021.814709>.
 34. Berthelot, J.M., Drouet, L., and Lioté, F. (2020). Kawasaki-like diseases and thrombotic coagulopathy in COVID-19: delayed over-activation of the STING pathway? *Emerg. Microbes Infect.* 9, 1514–1522. <https://doi.org/10.1080/22221751.2020.1785336>.
 35. Guo, L., and Rondina, M.T. (2019). The era of thromboinflammation: platelets are dynamic sensors and effector cells during infectious diseases. *Front. Immunol.* 10, 2204. <https://doi.org/10.3389/fimmu.2019.02204>.
 36. Cai, X., Chiu, Y.H., and Chen, Z.J. (2014). The cGAS-cGAMP-STING pathway of cytosolic DNA sensing and signaling. *Mol. Cell* 54, 289–296. <https://doi.org/10.1016/j.molcel.2014.03.040>.
 37. Zhang, H., Zeng, L., Xie, M., Liu, J., Zhou, B., Wu, R., Cao, L., Kroemer, G., Wang, H., Billiar, T.R., et al. (2020). TMEM173 drives lethal coagulation in sepsis. *Cell Host Microbe* 27, 556.e6–570.e6. <https://doi.org/10.1016/j.chom.2020.02.004>.
 38. Rendu, F., and Brohard-Bohn, B. (2001). The platelet release reaction: granules' constituents, secretion and functions. *Platelets* 12, 261–273. <https://doi.org/10.1080/09537100120068170>.
 39. Yadav, S., and Storrie, B. (2017). The cellular basis of platelet secretion: emerging structure/function relationships. *Platelets* 28, 108–118. <https://doi.org/10.1080/09537104.2016.1257786>.
 40. Chen, Y.A., and Scheller, R.H. (2001). SNARE-mediated membrane fusion. *Nat. Rev. Mol. Cell Biol.* 2, 98–106. <https://doi.org/10.1038/35052017>.
 41. Al Hawas, R., Ren, Q., Ye, S., Karim, Z.A., Filipovich, A.H., and Whiteheart, S.W. (2012). Munc18b/STXBP2 is required for platelet secretion. *Blood* 120, 2493–2500. <https://doi.org/10.1182/blood-2012-05-430629>.
 42. Ye, S., Karim, Z.A., Al Hawas, R., Pessin, J.E., Filipovich, A.H., and Whiteheart, S.W. (2012). Syntaxin-11, but not syntaxin-2 or syntaxin-4, is required for platelet secretion. *Blood* 120, 2484–2492. <https://doi.org/10.1182/blood-2012-05-430603>.
 43. Ma, Z., and Damania, B. (2016). The cGAS-STING defense pathway and its counteraction by viruses. *Cell Host Microbe* 19, 150–158. <https://doi.org/10.1016/j.chom.2016.01.010>.
 44. Margolis, S.R., Wilson, S.C., and Vance, R.E. (2017). Evolutionary origins of cGAS-STING signaling. *Trends Immunol.* 38, 733–743. <https://doi.org/10.1016/j.it.2017.03.004>.
 45. Decout, A., Katz, J.D., Venkatraman, S., and Ablasser, A. (2021). The cGAS-STING pathway as a therapeutic target in inflammatory diseases. *Nat. Rev. Immunol.* 21, 548–569. <https://doi.org/10.1038/s41577-021-00524-z>.
 46. Hopfner, K.P., and Hornung, V. (2020). Molecular mechanisms and cellular functions of cGAS-STING signalling. *Nat. Rev. Mol. Cell Biol.* 21, 501–521. <https://doi.org/10.1038/s41580-020-0244-x>.
 47. Amaral, A., Opal, S.M., and Vincent, J.L. (2004). Coagulation in sepsis. *Intensive Care Med.* 30, 1032–1040. <https://doi.org/10.1007/s00134-004-2291-8>.
 48. Giustozzi, M., Ehrlicher, H., Bongiovanni, D., Borovac, J.A., Guerreiro, R.A., Gąsecka, A., Papakonstantinou, P.E., and Parker, W.A.E. (2021).

- Coagulopathy and sepsis: pathophysiology, clinical manifestations and treatment. *Blood Rev.* 50, 100864. <https://doi.org/10.1016/j.blre.2021.100864>.
49. Akinosoglou, K., and Alexopoulos, D. (2014). Use of antiplatelet agents in sepsis: a glimpse into the future. *Thromb. Res.* 133, 131–138. <https://doi.org/10.1016/j.thromres.2013.07.002>.
50. Xu, Y., Jiang, H., Li, L., Chen, F., Liu, Y., Zhou, M., Wang, J., Jiang, J., Li, X., Fan, X., et al. (2020). Branched-chain amino acid catabolism promotes thrombosis risk by enhancing Tropomodulin-3 propionylation in platelets. *Circulation* 142, 49–64. <https://doi.org/10.1161/CIRCULATIONAHA.119.043581>.
51. Wang, J., Hossain, M., Thanabalasuriar, A., Gunzer, M., Meininger, C., and Kubes, P. (2017). Visualizing the function and fate of neutrophils in sterile injury and repair. *Science* 358, 111–116. <https://doi.org/10.1126/science.aam9690>.
52. Yang, X., Cheng, X., Tang, Y., Qiu, X., Wang, Y., Kang, H., Wu, J., Wang, Z., Liu, Y., Chen, F., et al. (2019). Bacterial endotoxin activates the coagulation cascade through gasdermin D-dependent phosphatidylserine exposure. *Immunity* 51, 983.e6–996.e6. <https://doi.org/10.1016/j.immuni.2019.11.005>.
53. Flevaris, P., Li, Z., Zhang, G., Zheng, Y., Liu, J., and Du, X. (2009). Two distinct roles of mitogen-activated protein kinases in platelets and a novel Rac1-MAPK-dependent integrin outside-in retractile signaling pathway. *Blood* 113, 893–901. <https://doi.org/10.1182/blood-2008-05-155978>.
54. Brigidi, G.S., and Bamji, S.X. (2013). Detection of protein palmitoylation in cultured hippocampal neurons by immunoprecipitation and acyl-biotin exchange (ABE). *J. Vis. Exp.* 50031. <https://doi.org/10.3791/50031>.
55. Aburima, A., Berger, M., Spurgeon, B.E.J., Webb, B.A., Wraith, K.S., Febbraio, M., Poole, A.W., and Naseem, K.M. (2021). Thrombospondin-1 promotes hemostasis through modulation of cAMP signaling in blood platelets. *Blood* 137, 678–689. <https://doi.org/10.1182/blood.2020005382>.
56. Jiang, H., Yu, Z., Ding, N., Yang, M., Zhang, L., Fan, X., Zhou, Y., Zou, Q., Hou, J., Zheng, J., et al. (2020). The role of AGK in thrombocytopoiesis and possible therapeutic strategies. *Blood* 136, 119–129. <https://doi.org/10.1182/blood.2019003851>.

STAR★METHODS

KEY RESOURCES TABLE

REAGENT or RESOURCE	SOURCE	IDENTIFIER
Antibodies		
Rabbit anti-STING	Cell Signaling Technology	Cat# 13647; RRID: AB_2732796
Mouse anti-STXBP2	Proteintech	Cat# 66238-1-Ig; RRID: AB_2881627
Rabbit anti-flag	Proteintech	Cat# 20543-1-AP; RRID: AB_11232216
Rabbit anti-HA	Proteintech	Cat# 51064-2-AP; RRID: AB_11042321
Mouse anti-beta actin	Abcam	Cat# ab8226; RRID: AB_306371
Rabbit anti-TBK1	Cell Signaling Technology	Cat# 3504; RRID: AB_2255663
Rabbit anti-P-TBK1	Cell Signaling Technology	Cat# 5483; RRID: AB_10693472
Rabbit anti-P-STING	Cell Signaling Technology	Cat# 85735; RRID: AB_2801279
Rabbit anti-IRF3	Proteintech	Cat# 11312-1-AP; RRID: AB_2127004
Rabbit anti-P-IRF3	Cell Signaling Technology	Cat# 37829; RRID: AB_2799121
Rabbit anti-Syntaxin11	Proteintech	Cat# 13301-1-AP; RRID: AB_2198214
Rabbit anti-SNAP23	Proteintech	Cat# 10825-1-AP; RRID: AB_2192022
Rabbit anti-VAMP8	Abcam	Cat# ab76021; RRID: AB_1310798
Mouse anti-Ubiquitin	Santa Cruz Biotechnology	Cat# sc-8017; RRID: AB_628423
Rabbit anti-SUMO2/3	Cell Signaling Technology	Cat# 4971; RRID: AB_2198425
Rat anti-CD42c	Emfret	Cat# M050-0
Normal Rabbit IgG	Cell Signaling Technology	Cat# 2729; RRID: AB_1031062
Mouse mAb IgG1	Cell Signaling Technology	Cat# 5415; RRID: AB_10829607
HRP-Streptavidin	Beyotime Biotechnology	Cat# A0303
HRP-anti-mouse IgG (H+L)	Jackson	Cat# 115-035-003; RRID: AB_10015289
HRP-anti-rabbit IgG (H+L)	Jackson	Cat# 111-035-003; RRID: AB_2313567
Rabbit anti-HistoneH3 (citulline R2+R8+R17)	Abcam	Cat# ab5103; RRID: AB_304752
Rabbit anti-STING	Proteintech	Cat# 19851-1-AP; RRID: AB_10665370
Rat anti-mouse CD62P	BD Biosciences	Cat# 553741; RRID: AB_395023
Rat anti-mouse IgG1	BD Biosciences	Cat# 559157; RRID: AB_397198
Rhodamine conjugated phalloidin antibody	Thermo Fisher	Cat# R415; RRID: AB_2572408
Mouse anti-alpha-Tubulin	Sigma-Aldrich	Cat# T5168; RRID: AB_477579
Rabbit anti-MPO	Thermo Fisher	Cat# PA5-16672; RRID: AB_11006367
Anti-GP1b β -DyLight649	Emfret	Cat# X-649; RRID: AB_2861336
Anti-mouse IgG (H+L)-Alexa Fluor (R) 488	Jackson	Cat# 115-545-146; RRID: AB_2307324
Anti-rabbit IgG (H+L)-Alexa Fluor (R) 647	Thermo Fisher	Cat# A-21244; RRID: AB_2535812
Anti-rabbit IgG (H+L)- Rhodamine (TRITC)	Jackson	Cat# 111-025-003; RRID: AB_2337926
Anti-mouse P-selectin-FITC	BD Biosciences	Cat# 553744; RRID: AB_395026
Anti-mouse JON/A-PE	Emfret	Cat# M023-2; RRID: AB_2833084
PAC-1 antibody-FITC	Thermo Fisher	Cat# MA5-28564; RRID: AB_2745523
Anti-human P-selectin-PE	BD Biosciences	Cat# 555524; RRID: AB_395910
Anti-mouse CD107a-FITC	Proteintech	Cat# FITC-65050; RRID: AB_2883740
Anti-mouse Ly-6G-Alexa Fluor (R) 488	BioLegend	Cat# 127626; RRID: AB_2561340
Anti-mouse CD41-APC	BioLegend	Cat# 133914; RRID: AB_11125581
Anti-mouse CD115-BV421	BioLegend	Cat# 135513; RRID: AB_2562667
Anti-mouse CD3epsilon-PE	BioLegend	Cat# 100308; RRID: AB_312673
Anti-mouse Ly-6G-Alexa Fluor (R) 647	BioLegend	Cat# 127609; RRID: AB_1134162
Anti-mouse CD154-PE	BioLegend	Cat# 106505; RRID: AB_313270
Streptavidin-APC	BD Biosciences	Cat# 554067; RRID: AB_10050396

(Continued on next page)

Continued

REAGENT or RESOURCE	SOURCE	IDENTIFIER
Chemicals, peptides, and recombinant proteins		
3'3'-cGAMP	InvivoGen	Cat# tlr1-nacga
H151	Selleck	Cat# S6652
DAPI	Yeasen	Cat# 40727ES10
FITC Dextran 2000	TdB Labs	Cat# FD2000
SYTOX Green	Thermo Fisher	Cat# S7020
Collagen	Chrono-log	Cat# P/N 385
Thrombin	Enzyme Research Laboratories	Cat# HT 1002a
Apyrase	Sigma-Aldrich	Cat# A6535
Prostaglandin E1	Sigma-Aldrich	Cat# P5515
Fibrinogen	Sigma-Aldrich	Cat# F3879
Anti-FLAG M2 affinity gel	Sigma-Aldrich	Cat# A2220
Western and IP Lysis Buffer	Beyotime Biotechnology	Cat# P0013
Tirofiban	Grand Pharmaceutical Group Limited	N/A
Sulfo-NHS-LC-Biotin	Thermo Fisher	Cat# 21335
Polymorphprep	Axis-Shield	Cat# 1114683
STING peptide (ST1-ST12)	GL Biochem Co., Ltd	N/A
Scrambled peptide: TGQAGHDQDKI	This Paper	N/A
ST5 peptide: QQTGDHAGIKD	This Paper	N/A
C-Scrambled peptide: GRKKRRQRRRTGQAGHDQDKI	This Paper	N/A
C-ST5 peptide: GRKKRRQRRRQQTGDHAGIKD	This Paper	N/A
Critical commercial assays		
ELISA kit for Platelet Factor4 (PF4)	Cloud-clone corp	Cat# SEA172Mu
ATP kit	Beyotime Biotechnology	Cat# S0026
Cell Death Detection ELISA	Roche	Cat# 11544675001
Mouse fibrinogen ELISA kit	Abcam	Cat# ab213478
Mouse Thrombin-Antithrombin Complexes ELISA kit	Abcam	Cat# ab137994
P-selectin ELISA kit	Thermo Fisher	Cat# EMSELP
CD40L (Soluable) ELISA kit	Thermo Fisher	Cat# BMS6010
LinKine™ AbFluor™ 488 Labeling kit	Abbkine	Cat# KTL0520
Experimental models: Cell lines		
HEK293T	Cell bank of the Chinese academy of sciences	N/A
Experimental models: Organisms/strains		
C57BL/6 mice	Shanghai SLAC Laboratory Animal Co., Ltd.	N/A
<i>Sting</i> ^{fl/fl} mice	GemPharmatech Co., Ltd	N/A
<i>Platelet factor 4 (P4)-Cre</i> mice	The Jackson Laboratory	Cat# 008535; RRID: IMSR_JAX:008535
Oligonucleotides		
Primer: PCR assay of STING Forward: 5' TCCCAGGGTGAGCTTTGTTAAAG 3'	This Paper	N/A
Primer: PCR assay of STING Reverse: 5' GGAGTTGGATC ATGCTCACTGATC 3'	This Paper	N/A
Primer: PCR assay of PF4 Forward: 5' CCCATACAGCATACCTTTTG 3'	This Paper	N/A
Primer: PCR assay of PF4 Reverse: 5' TGCACAGTCAGCAGGTT 3'	This Paper	N/A

(Continued on next page)

Continued

REAGENT or RESOURCE	SOURCE	IDENTIFIER
Software and algorithms		
Graphpad Prism	Graphpad software	N/A
Image J	NIH	N/A
FlowJo	Three Star	N/A
Adobe Photoshop CS6	Adobe	N/A
NIS Elements software	Nikon Instruments	N/A
RStudio	N/A	https://www.rstudio.com/

RESOURCE AVAILABILITY

Lead contact

Further information and requests for resources and reagents should be directed to and will be fulfilled by the lead contact, Yanyan Xu (xuyanyan901@shsmu.edu.cn).

Materials availability

This study did not generate new unique reagents.

Data and code availability

All data reported in this paper will be shared by the [lead contact](#) upon reasonable request. This study did not generate any unique dataset or code.

EXPERIMENTAL MODEL AND SUBJECT DETAILS

Mice

The *Sting*-floxed mice (Strain NO. T009704) were constructed by GemPharmatech Co., Ltd (Nanjing, China). Clustered regularly interspaced short palindromic repeats (CRISPR)-associated protein (Cas) technology was used to knock out the target sequence at exon 1 to exon 8 of the *Sting*-201 (ENSMUST00000115728.4) transcript on the *C57BL/6* genetic background. The floxed mice were subjected to knockout after mating with mice expressing Cre recombinase (008535, *Pf4-Cre*; The Jackson Laboratory), resulting in STING deletion in megakaryocytes/platelets. As a result, megakaryocyte/platelet STING knockout mice (*Sting*^{fl/fl} *pf4-Cre*⁺, *Sting*^{-/-}) and control mice (*Sting*^{fl/fl} *pf4-Cre*⁻, *Sting*^{fl/fl}) were obtained. The mice were genotyped via polymerase chain reaction (PCR), and STING deficiency in platelets was confirmed by western blotting. All experimental mice were mated and reproduced under specific pathogen-free (SPF) conditions. 6–8 weeks old mice were used for all experiments without sex bias. The Shanghai Jiao Tong University School of Medicine Animal Care and Use Committee approved the animal research.

Sepsis Model: Cecal Ligation and Puncture (CLP) Assay

CLP operation was performed as previously described.²⁵ Briefly, 75% medical alcohol was used to disinfect the mouse abdomen, and CLP surgery was conducted under isoflurane with oxygen. For the polymicrobial sepsis model, the cecum of the subjects was partially ligated and then punctured with a 22-gauge needle. After puncturing, an equal amount of feces was squeezed out, and the cecum was then placed back into the abdominal cavity. The wound was stitched, and the mice were injected with 1 mL of sterile saline immediately after surgery. Mouse survival was observed and recorded for 7 days after surgery. The sham group was subjected to the same surgical procedure without ligation and puncture. None of the experimental mice received antibiotics.

Hemostasis Model: Mouse Tail Bleeding Assay

To evaluate hemostasis, the bleeding time assay was performed as previously described.⁵⁰ Briefly, mice were anesthetized, and a 3 mm section of the tail tip was amputated. The injured tail was immediately immersed in 0.9% NaCl maintained at 37 °C, and the bleeding time was recorded.

Arterial Thrombosis Model: FeCl₃-induced Carotid Artery Injury Assay

To evaluate arterial thrombosis, a ferric chloride-induced carotid artery injury murine thrombosis model was implemented as described previously.⁵⁰ Thrombus formation was continuously monitored for 20 minutes and the time of occlusion was recorded.

Vein Thrombosis Model: Inferior Vena Cava (IVC) Stenosis Assay

To evaluate vein thrombosis, the inferior vena cava stenosis model was performed as previously described.⁵⁰ Mice were anesthetized with 1% Nembutal and the IVC was ligated over a 31-g blunt needle with a 7.0 polypropylene suture. Forty-eight hours later, the IVC and the associated thrombus, were harvested, photographed, weighed and measured for thrombus length.

METHOD DETAILS

Preparation for Intravital Microscopy (IVM)

Intraperitoneal injection of Avertin (2.5%) was used to anesthetize the sham and CLP group mice. Then, the antibodies were injected via the tail vein after anesthetization. Surgical preparation of the mouse liver for intravital imaging was performed as previously described.⁵¹ Briefly, the liver was exposed from the abdomen to the chest along an intermediate using an electrocoagulation knife. Then, the left liver was fixed on a glass coverslip with dust-free paper soaked in PBS. Images and videos were acquired using IVM. Surgical preparation of the mouse lung for intravital imaging was performed as previously described.⁵¹ Briefly, the trachea was exposed to attach the ventilator for tracheal intubation after anesthesia. Then, the left lung was exposed to generate a window for imaging. A special suction chamber with a glass slide attached to the exposed lung surface was used to obtain mouse lung images and videos. The suction was stabilized at 20–30 mm Hg.

IVM and Image Analysis

Liver images were acquired using an inverted Olympus FV3000 confocal microscope. The microscope was driven by FV31S software. A 20X N.A. 0.75 UPLANSAPO objective lens was used to capture images. Three laser excitation wavelengths (488, 561, and 647 nm) were used for liver visualization. HyD or PMT detectors were used for fluorescence detection. Platelets and blood flow were visualized by injection of the DyLight649-GP1b β antibody (0.1 μ g/g) and dextran 2000 (10 μ g/g). NETs were visualized by using the Alexa Fluor 594 anti-mouse Ly-6G antibody (0.5 μ g/g), the Alexa Fluor 488 anti-mouse citrullinated histone H3 antibody (0.5 μ g/g), and the DyLight649-GP1b β antibody (0.1 μ g/g). Image analysis methods were performed as previously described.⁵² Acquired images were analyzed using ImageJ software. For occlusive vessels, all results were presented as the percentage of occlusive vessel area to the whole area. For platelets, all results were presented as the percentage of positively stained (DyLight649-GP1b β -dark red) area to the whole area. The same parameters were used for all image analyses.

Multiphoton Laser Scanning Confocal Intravital Microscopy

Olympus multiphoton imaging system (FVMPE-RS, Tokyo, Japan) was used to capture images of the exposed left lung. A 25x/NA 1.05 water objective was used to capture images. The microscope system was equipped with a multiphoton light path based on an upright microscope (BX63, Olympus), and a tunable femtosecond pulse laser (MaiTaiDeepSee, Spectra Physics, USA). Three laser excitation wavelengths (488, 561, and 647 nm) were used for lung visualization. Image analysis were performed as described above.

Biochemical Assays and Lung Function Assays

Blood was obtained from *Sting*^{ff} and *Sting*^{-/-} mice, and blood cell counts were analyzed with an autoanalyzer (Sysmex, XN-1000V-B1). Plasma was obtained by centrifugation at 3000 \times g for 10 minutes. The plasma levels of ALT were detected using a BECKMAN automatic biochemistry analyzer (BECKMAN, Brea, CA, USA). Inspiratory resistance and expiratory resistance were measured with the AniRes2005 Lung Function System (version 2.0; Bestlab Technology Co.) according to the manufacturer's instructions.

Measurement of Neutrophil-Platelet and Monocyte-Platelet Aggregation

Samples of mouse orbital blood were collected at different time points after sham and CLP surgery, and anticoagulated whole blood was then lysed with red blood cell lysate buffer (0.15 M NH₄Cl, 1 mM NaHCO₃, 0.1 mM EDTA, pH=7.25) at room temperature for 10 minutes. After lysing, the samples were centrifuged at 400 \times g for 5 minutes to obtain the supernatant for flow cytometry staining. Anti-mouse CD41-APC, anti-mouse Ly6G-Alexa Fluor 488 and anti-mouse CD115-BV421 antibodies were used to label platelets, neutrophils, and monocytes, respectively. All samples were kept at 4°C for 30 minutes and analyzed using flow cytometry (Beckman CytoFlex S).

Platelet Preparation, Aggregation, P-selectin Exposure, JON/A Binding, PAC1 Binding, Spreading, and Clot Retraction

The preparation and stimulation of human and mouse platelets were performed as described previously.⁵⁰ For the platelet aggregation assay, 300 μ L 3 \times 10⁸/mL platelets were used in response to collagen and thrombin. Platelets were incubated with the PE-conjugated JON/A antibody (mouse), FITC-conjugated PAC1 antibody (human), FITC-conjugated P-selectin antibody (mouse) or PE-conjugated P-selectin antibody (human) in the presence of thrombin for 20 minutes at room temperature. The levels of P-selectin exposure, JON/A binding and PAC1 binding were measured using flow cytometry. Platelet spreading on immobilized fibrinogen was completed as described previously.⁵⁰ Platelets were stained using rhodamine-conjugated phalloidin and visualized with a microscope (ZEISS 880). Five images were chosen at random and analyzed with ImageJ. Clot retraction was conducted as previously described.⁵³ The level of clot retraction was evaluated using ImageJ.

Platelet Secretion Analysis

For PF4 and ATP assays, platelet samples were collected after aggregation. The samples containing 5 mM EDTA were centrifuged for 10 minutes at 2100 rpm at 4°C to acquire the supernatants. For the PF4 ELISA, supernatant samples were diluted 1:200 and evaluated using the ELISA Kit of Platelet Factor 4. For the ATP assay, samples (1:20 dilution) were evaluated using the ATP Assay Kit.

Manipulation was performed according to the guidance of manufacturer. For the LAMP1 assay, platelets were incubated with the FITC-anti-mouse LAMP1 antibody in the presence of thrombin for 20 minutes at room temperature and the level of LAMP1 expression was analyzed using flow cytometry.

Transmission Electron Microscopy (TEM) and Immunoelectron Microscopy (IEM)

For TEM, 4% glutaraldehyde in phosphate buffer (0.1 M, pH 7.4) was used to fix mouse platelets for 2 hours. Then, 2% osmium tetroxide was used to further fix the platelets after removing phosphate buffer. Platelets were embedded in epon and 2% uranyl acetate and lead citrate were used to stain the slices. Images were acquired with a CM-120 transmission electron microscope (FEI, OR, USA). For IEM, isolated human platelets were fixed in 3% formaldehyde-0.5% glutaraldehyde in 0.1 M phosphate buffer (pH 7.2). Platelets were incubated with anti-STING polyclonal antibodies for immunogold staining. The images were acquired with a FEI Talos L120C. Platelet α -granules and dense granules were counted in randomly fields of view.

Protein-Protein Docking

Protein Data Bank (PDB): 6NT5 and 4CCA were selected as the starting models for STING and STXBP2. Molecular docking was performed by means of a protein-protein docking protocol (<https://answers.illinois.edu/scs/page.php?id=104084>). Two models were refined to reasonable conformation after supplementing missing residues with reference to AlphaFold2 predicted structures. All non-amino acid atoms, such as water and salt ions, were removed from both structures using Quick-Preparation in Molecular Operating Environment (MOE). The 137-301 residues of STING were chosen to be the contact region, while there were no restrictions on STXBP2. An ideal binding mode was selected based on the findings of biological studies and the ranking scores. The final structure after molecular dynamics simulation was analyzed with a PISA interface sever. Molecular graphics were generated with PyMOL.

ELISA

The relative binding levels of ST1-12 to STXBP2 were measured by ELISA. Briefly, ST1-12 peptides were synthesized and used to coat 96-well plates overnight at 4°C. After being washed 3 times using PBST, HEK293T cell lysates transfected with STXBP2-HA were added to 96-well plates and incubated at 37°C for 2 hours. After washing, the anti-HA antibody was added and incubated at 37°C for 1 hour. The horseradish peroxidase (HRP) anti-rabbit antibody and 3,3',5,5'-tetramethylbenzidine (TMB) were used to detect anti-HA antibody. Finally, 2 M sulfuric acid was added to terminate color development, and the absorbance was assayed at 450 nm. Levels of plasma fibrinogen, TAT, sCD62P and sCD40L were measured using ELISA as suggested by the manufacturer.

NETosis Experiment *In Vitro*

Platelet-induced NETosis was performed as previously described.²⁷ Briefly, anticoagulated whole blood was obtained from healthy volunteers, and then platelets and neutrophils were then isolated as previously described.^{27,50} Platelets, which were preincubated with C-ST5 peptides or C-scrambled peptides for 1 hour at 37°C, were then mixed with neutrophils and 0.2 U/mL thrombin for 2 hours at 37°C and 5% CO₂. The adherent cells were fixed with 4% paraformaldehyde for immunofluorescence staining.

NET quantification in the cell culture supernatant was performed by using MPO-DNA ELISA.²⁷ Briefly, the myeloperoxidase polyclonal antibody was used to coat 96-well plates overnight at 4°C. Then, 20 μ L of supernatant sample plus 80 μ L of incubation buffer including anti-DNA-POD was incubated in myeloperoxidase polyclonal antibodies coated 96-well plates and shaken for 2 hours at 300 rpm and 25°C the next day. Finally, peroxidase substrate (ABTS) was added to the 96-well plates and incubated for 20 minutes in the dark at room temperature. The MPO-DNA level was determined based on the absorbance measured at 405-nm according to the manufacturer's protocol.

Acyl-Biotin Exchange (ABE) Palmitoylation Assay

The assay was performed as previously described.⁵⁴ In brief, platelets were lysed using lysis buffer (1% NP-40, 10% glycerol, 50 mM Tris-HCl pH 7.5, 150 mM NaCl, and protease inhibitor) supplemented with 50 mM N-ethylmaleimide (NEM). Cell lysates were centrifuged at 12000 \times g for 15 minutes. Platelet STING was enriched via IP with anti-STING antibodies. The thioester bond of palmitoyl was hydrolyzed using 1 M hydroxylamine (HAM) and replaced by biotin-BMCC. Ultimately, the palmitoylated target protein was identified by immunoblotting with streptavidin-HRP. A control group that did not receive HAM treatment was also included.

Platelet Transfusion Assay

Platelet transfusion assay was performed as previously described.⁵⁵ Platelets were enriched from *Sting*^{fl/fl} and *Sting*^{-/-} mice, and they were injected into 6~8-week-old *WT* mice by the tail veins (5 \times 10⁸ platelets/per mouse). After injection, CLP operation was performed and the processes of thrombosis in the liver were recorded.

Platelet Lifespan Assay

Platelet lifespan assays were performed as previously described.⁵⁶ Briefly, mice were injected with Sulfo-NHS-LC-Biotin intravenously, and orbital blood was collected at different time points. Biotin positive platelets were identified with APC-streptavidin by flow cytometry.

Plasmid Construction and Plasmid Transfection

The human STING full length sequence, STING truncated sequence, and human STXBP2 sequence were PCR amplified from HEK293T cell complementary DNA and cloned into vectors P-FLAG-CMV, P-FLAG-CMV and pXJ40-hemagglutinin (HA), respectively. Plasmids were transfected into HEK293T cells using Lipo2000, and the cells were lysed in Western and IP Lysis Buffer at 48 hours post-transfection.

The Synthesis of Peptides

Peptides were synthesized by Fmoc Solid Phase Peptide Synthesis (SPPS) method. Briefly, DCM was used to swell the 2-Chlorotrityl Chloride Resin (1.05 mmol/g, substitution). Then, in the presence of DIEA, the amino acid coupling was carried out for 45 minutes using 3× excess amino acid and HBTU. The ninhydrin test was used to keep track of the generation and consumption of free primary amine. The deprotection and coupling procedure was carried out repeatedly until the necessary length of peptide was produced. The cleavage solution (95% TFA, 1% water, 2% EDT, and 2% TIS) was used to obtain the cleaved conjugate. Cold ether was then used to precipitate the cleaved conjugate. And ACD and H₂O were used to dissolve the crude peptide product. We used HPLC and mass spec system to qualitatively analyze and purify the peptide. After validation, the mature peptides were finally obtained by purifying and lyophilizing.

Immunoprecipitation (IP)

After transfection with plasmid for 48 hours, HEK293T cells were lysed by using Western and IP Lysis Buffer with protease inhibitor for 30 minutes at 4°C. Then the cell suspension was centrifuged for 15 minutes at 12000 rpm at 4°C to obtain the supernatant. Flag agarose beads were added to bind the target protein overnight at 4°C. The agarose beads were harvested and washed 3 times the next day.

For endogenous IP, platelets were lysed in 1% NP40 and the cell lysate was incubated with indicated antibodies or control IgG at 4°C overnight. The next day, protein A/G agarose beads were added to the suspension and incubated at 4°C for 2 hours, and the beads were then harvested and all samples were evaluated by western blotting.

Immunofluorescence and Confocal Microscopy

Human platelets were prepared as described previously.⁵⁰ For platelet immunofluorescence staining, platelets were cultured on cover slips coated with 50 μg/mL fibrinogen at 37°C and then spreading platelets were fixed in 4% paraformaldehyde for 10 minutes at room temperature. Fixed platelets were permeabilized in 0.2% Triton X-100 and blocked in 2% bovine serum albumin (BSA). After blocking, platelets were stained with anti-STING and anti-STXBP2 antibodies. Immunofluorescence images were captured using a laser scanning confocal microscope (ZEISS, LSM 880) on the platform of Shanghai Jiao Tong University School of Medicine, and the 100× lens oil lens was used to obtain images. The images were analyzed using ZEN imaging software (Carl Zeiss, GmbH). For *in vitro* NETosis immunofluorescence staining, the anti-citrullinated histone H3 antibody and DAPI were used. The images were captured as described above.

QUANTIFICATION AND STATISTICAL ANALYSIS

Statistical analyses were performed with GraphPad Prism 7.0. Data are presented as the mean ± standard error of the mean (SEM). An unpaired *t* test was used for comparisons between two conditions. For multiple comparisons, one-way ANOVA or two-way ANOVA was performed. Survival results were analyzed using the log-rank test. Values of $p \leq 0.05$ were considered statistically significant.